Engineering Fracture Mechanics Vol. 43, No. 2, pp. 217–255, 1992
Printed in Great Britain.

0013-7944/92 $5.00 + 0.00

STRESSES AND DISPLACEMENTS AROUND CRACKS AND ELLIPTICAL CAVITIES: EXACT SOLUTIONS

D. MAUGIS

Laboratoire mixte des matériaux et des structures de génie civil, LCPC/CNRS,
58 Bd Lefebvre, 75732 Paris Cédex 15, France

Abstract—The stress tensor given by Chang and Wu [*J. appl. Mech.* **47**, 57–63 (1980)] is depicted by drawing contours of principal stresses, isopachics, isochromatic lines, the von Mises criterion and stress trajectories for both elliptical cavities and cracks under uniaxial or biaxial loading. For cracks it is written in Cartesian coordinates, and simple expressions are given for mode I.

Published experimental results on angled cracks are in agreement with the slope of the stress trajectory starting from the crack tip or the more stressed point of the cavity.

The Stevenson [*Proc. R. Soc.* **A184**, 129–179 (1945)] complex potentials, proper for stresses, are not suitable for displacements, since they lead to a rotation at infinity. Correct potentials in elliptical coordinates are derived from the Muskhelishvili potentials in conformal representation, and the displacement field around cavities or cracks is depicted. The shape of the deformed crack is in agreement with the one directly computed by Theocaris *et al.* [*Int. J. Fracture* **30**, 135–153 (1986)]. However, in the framework of linearized elasticity, no conclusion can be drawn on the overlapping of crack lips found by the exact calculation when it is due to a second order effect.

1. INTRODUCTION

In 1913, Inglis [1] calculated the stress tensor around an elliptical cavity (major and minor axes $2a$ and $2b$) traversing a plate. The stress tensor was very simple in the case of a plate subjected to a tensile stress σ in all directions, and this tensor was used later by Griffith [2] in his famous theory. In the case of a plate subjected to uniaxial stress σ with an inclined ellipse (angle β between the major axis and the stress σ) the stress tensor, as given by Inglis, was rather complicated and given in the form of infinite series.

The problem of the elliptical cavity was further examined by Pöschl [3], Wolf [4], Muskhelishvili [5, 6], Föpl [7], Stevenson [8], Timoshenko and Goodier [9] and Neuber [10]. For uniaxial loading the complex potentials were given by Muskhelishvili using conformal mapping and by Stevenson using elliptical coordinates. The Stevenson complex potentials were used by Jaeger and Cook [11], and later by Wu and Chang [12, 13], who derived the stress tensor for uniaxial and biaxial loadings. However, the Stevenson complex potentials, although correct for stresses, are not suitable (for a term is missing) and lead to wrong results for displacements. The correct expressions are given in the present paper. The complete state of stresses around an elliptical cavity was never depicted. To our knowledge, only isochromatic lines were given by Küppers [14] in the special case $a/b = 500$, and $\beta = \pi/2$ from the Inglis stress tensor for uniaxial loading.

For a crack whose lips are assumed to be interaction-free the leading terms of the series expansion of stresses and displacements were given independently by Sneddon [15] from the Westergaard [16] solution and by Williams [17]. It soon appeared that the singular terms were insufficient to evaluate the stress intensity factors from isochromatic fringes [18] and Irwin [19] proposed to use the constant second term in the series to improve the accuracy. The history of the constant term is rather complicated. It did not appear in [15] and [17] and was subtracted from σ_x by Irwin [20] in an obscure fashion for uniaxial loading. In fact Sih [21], Eftis and Liebowitz [22] and Eftis *et al.* [23] pointed out that a real constant term was lacking in the Westergaard equations, and that for a biaxial loading (σ perpendicular to the crack, $k\sigma$ parallel to the crack) the quantity $(1-k)\sigma$ must be subtracted from σ_x. The inclined crack under biaxial loading (angle β between the crack and σ) was studied by Eftis and Subramonian [24] who showed that stress intensity factors depend on the horizontal load parameter k:

$$K_I = \tfrac{1}{2}(m - n\cos 2\beta)\sigma\sqrt{(\pi a)} \tag{1}$$

$$K_{II} = \tfrac{1}{2}n \sin 2\beta\, \sigma\sqrt{(\pi a)}, \tag{2}$$

where $m = 1 + k$, $n = 1 - k$, and that the constant term was $n \cos 2\beta$. Later the three-term series expansion was given by Theocaris and Spyropoulos [25] in order to improve the accuracy of isochromatic lines. The influence of the constant term of the series expression on the crack path stability was pointed out by Cotterell [26], and further discussed by Cotterell and Rice [27] and Sumi *et al.* [28, 29].

Concerning the displacement field only the exact shape of a crack was studied by Theocaris [30–34] and Theocaris *et al.* [35–37], and the exact shape of isopachics by Theocaris [38]. In particular the rotation of the crack, in mixed-mode, and the crack flanks overlapping in mode II, were pointed out.

In the present paper the exact solution for stresses around an elliptical cavity as derived by Chang and Wu [13] is thoroughly investigated: contours of principal stress, von Mises criterion, isochromatic lines, and stress trajectories are given. For cracks, formulas are relatively simple and easier to use than three-term approximations.

The exact solution for the displacement field is derived, from the Muskhelishvili [6] solution, and for a crack the elastic displacements along the flanks are in agreement with those directly computed by Theocaris *et al.*

2. ELLIPTICAL COORDINATES

Let us consider a homogeneous and isotropic infinite plate subjected to a biaxial loading σ along Oy' and $k\sigma$ along Ox'. This plate contains a stress-free elliptical cavity (semi-axis a and $b < a$) whose major axis Ox makes an angle β with the Oy' axis. Coordinates x and y will thus refer to the axis of the ellipse.

Elliptical coordinates are defined by

$$x = c \cosh \xi \cos \eta \tag{3}$$

$$y = c \sinh \xi \sin \eta, \tag{4}$$

where $c > 0$, $\xi \geqslant 0$, $0 \leqslant \eta \leqslant 360°$. (Note that the x-axis is defined by $\xi = 0$ for $|x| < c$ and by $\sin \eta = 0$ for $|x| > c$.) Eliminating ξ or η, we obtain

$$\frac{x^2}{c^2 \cosh^2 \xi} + \frac{y^2}{c^2 \sinh^2 \xi} = 1 \tag{5}$$

$$\frac{x^2}{c^2 \cos^2 \eta} - \frac{y^2}{c^2 \sin^2 \eta} = 1. \tag{6}$$

At constant ξ or η, these two equations describe, respectively, homofocal ellipses or hyperbolas, as shown in Fig. 1. The elliptical cavity is defined by $\xi = \xi_0$, with $a = c \cosh \xi_0$ and $b = c \sinh \xi_0$, hence

$$c^2 = a^2 - b^2. \tag{7}$$

Some useful relations between coordinates x, y and ξ, η are given in Appendix 1.

3. COMPLEX POTENTIALS

The Kolosov–Muskhelishvili relations [6] are

$$\sigma_x + \sigma_y = 2[\varphi'(z) + \overline{\varphi'(z)}] = 4 \operatorname{Re} \varphi'(z) \tag{8}$$

$$\sigma_y - \sigma_x + 2i\tau_{xy} = 2[\bar{z}\varphi''(z) + \chi''(z)] \tag{9}$$

$$2\mu(u_x + iu_y) = \kappa\varphi(z) - z\overline{\varphi'(z)} - \overline{\chi'(z)}, \tag{10}$$

where $z = x + iy$, $\kappa = (3 - \nu)/(1 + \nu)$ for plane stress, $\kappa = 3 - 4\nu$ for plain strain (μ and ν are the shear modulus and the Poisson ratio, respectively). The first two will be written in elliptical coordinates [6] as

$$\sigma_\xi + \sigma_\eta = 4 \operatorname{Re} \varphi'(z) \tag{11}$$

$$\sigma_\eta - \sigma_\xi + 2i\tau_{\xi\eta} = 2\, e^{2i\alpha}[\bar{z}\varphi''(z) + \chi''(z)] \tag{12}$$

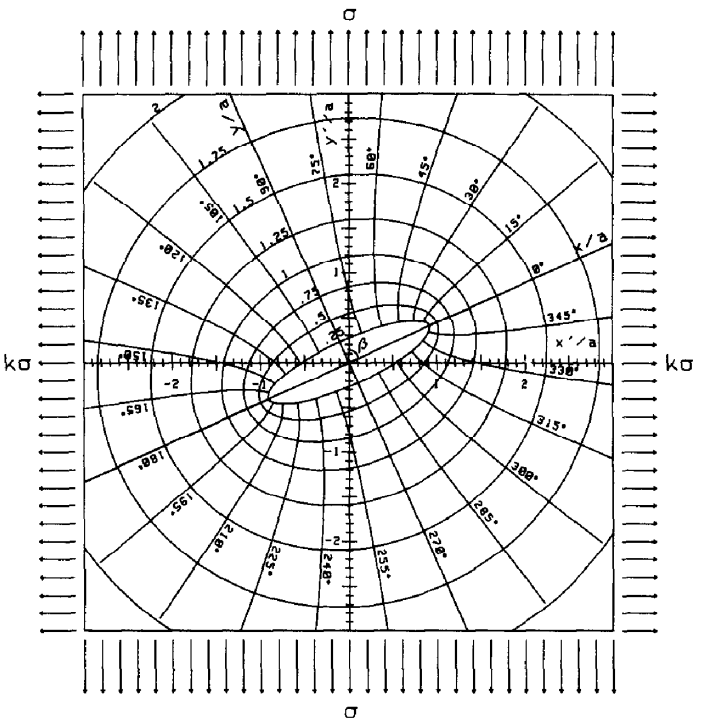

Fig. 1

where

$$e^{2i\alpha} = \frac{\sinh \zeta}{\sinh \bar{\zeta}} \tag{13}$$

$$z = x + iy = c \cosh(\xi + i\eta) = c \cosh \zeta. \tag{14}$$

The stresses σ_ξ and σ_η are perpendicular, respectively, to the ellipses and to the hyperbolas.

Complex potentials $\varphi(z)$ and $\chi(z)$ for uniaxial loading ($k = 0$) have been computed by Stevenson [8]. With this loading the boundary conditions at infinity are

$$\sigma_{y'} = \sigma$$

$$\sigma_{x'} = \tau_{x'y'} = 0,$$

whereas on the stress-free cavity one has

$$\sigma_\xi = \tau_{\xi\eta} = 0, \quad \xi = \xi_0.$$

(Note that compression of the flanks of the cavity is not allowed.) Stevenson has shown that these boundary conditions are satisfied by taking

$$4\varphi(z) = \sigma c[e^{2\xi_0} \cos 2\beta \cosh \zeta + (1 - e^{2\xi_0} e^{2i\beta}) \sinh \zeta] \tag{15}$$

$$4\chi(z) = -\sigma c^2[(\cosh 2\xi_0 - \cos 2\beta)\zeta + \tfrac{1}{2} e^{2\xi_0} \cosh 2(\zeta - \xi_0 - i\beta)]. \tag{16}$$

These potentials have frequently been used [9, 11, 12, 13] to compute stresses. However, they are not suitable for displacements since the condition of no rotation at infinity [6], $\operatorname{Im} \varphi'(z) \to 0$ when $|z| \to \infty$, is not satisfied.

This problem was initially studied by Muskhelishvili [6] using the conformal mapping:

$$z = R\left(\zeta_1 + \frac{m}{\zeta_1}\right), \quad R > 0, \quad 0 \leqslant m < 1,$$

where $a = R(1+m)$ and $b = R(1-m)$. Using the above boundary conditions for stresses, and imposing no rotation at infinity, he obtains:

$$\varphi(\zeta_1) = \frac{\sigma R}{4}\left(\zeta_1 + \frac{2\,e^{2i\beta} - m}{\zeta_1}\right) \tag{17}$$

$$\chi'(\zeta_1) = -\frac{\sigma R}{2}\left[e^{-2i\beta}\zeta_1 + \frac{e^{2i\beta}}{m\zeta_1} - \frac{(1+m^2)(e^{2i\beta} - m)}{m}\cdot\frac{\zeta_1}{\zeta_1^2 - m}\right]. \tag{18}$$

If we return to elliptical coordinates, with

$$R = \frac{c}{2}e^{\xi_0}$$

$$m = e^{-2\xi_0}$$

$$\zeta_1 = e^{-\xi_0}e^{\zeta},$$

eqs (17) and (18) can be rewritten as

$$4\varphi(z) = \sigma c[e^{2\xi_0}e^{2i\beta}\cosh\zeta + (1 - e^{2\xi_0}e^{2i\beta})\sinh\zeta] \tag{19}$$

$$4\chi'(z) = -\frac{\sigma c}{\sinh\zeta}[\cosh 2\xi_0 - \cos 2\beta + e^{2\xi_0}\sinh 2(\zeta - \xi_0 - i\beta)]. \tag{20}$$

Comparison with eqs (15) and (16) shows that $\cos 2\beta$ in eq. (15) must be replaced by $e^{2i\beta}$. (This coefficient was shown by Stevenson not to be pure imaginary and was taken as pure real.) This modification which corresponds to a rigid body rotation does not change the stress tensor where only $\mathrm{Re}\,\varphi'(z)$ and $\varphi''(z)$ appear.

By superposition one obtains the complex potentials for biaxial loading. We have to add to each expression the same expression with σ replaced by $k\sigma$ and β replaced by $\beta + \pi/2$. We obtain

$$4\varphi(z) = \sigma c[n\,e^{2\xi_0}e^{2i\beta}\cosh\zeta + (m - n\,e^{2\xi_0}e^{2i\beta})\sinh\zeta] \tag{21}$$

$$4\chi'(z) = -\frac{\sigma c}{\sinh\zeta}[m\cosh 2\xi_0 - n\cos 2\beta + n\,e^{2\xi_0}\sinh 2(\zeta - \xi_0 - i\beta)], \tag{22}$$

where

$$m = 1 + k$$

$$n = 1 - k.$$

Calculations are tedious, but we obtain

$$\frac{\sigma_\eta + \sigma_\xi}{\sigma} = B + \lambda(A\sinh 2\xi - C\sin 2\eta) \tag{23}$$

$$\frac{\sigma_\eta - \sigma_\xi}{\sigma} = -\lambda[\cosh 2(\xi - \xi_0) - 1](B\cos 2\eta + C\sin 2\eta) + \lambda(\cosh 2\xi_0 - \cos 2\eta)[B + \lambda(A\sinh 2\xi - C\sin 2\eta)] \tag{24}$$

$$\frac{2\tau_{\xi\eta}}{\sigma} = -(C + \lambda B\sin 2\eta)\sinh 2(\xi - \xi_0) + \lambda C\sinh 2\xi[\cosh 2(\xi - \xi_0) - 1] + \lambda^2(\cosh 2\xi - \cosh 2\xi_0)(A\sin 2\eta + C\sinh 2\xi) \tag{25}$$

$$u_x = \frac{\sigma c}{8\mu}[(\kappa+1)(A\sinh\xi\cos\eta + B\cosh\xi\cos\eta + C\,e^{-\xi}\sin\eta) - 4\sinh(\xi - \xi_0)\sinh\xi_0(B\cos\eta + C\sin\eta) - 2\lambda(\cosh 2\xi - \cosh 2\xi_0)(A\sinh\xi\cos\eta - C\cosh\xi\sin\eta)] \tag{26}$$

$$u_y = \frac{\sigma c}{8\mu}[(\kappa+1)(A\cosh\xi\sin\eta + B\sinh\xi\sin\eta + C\,e^{-\xi}\cos\eta)$$
$$- 4\sinh(\xi-\xi_0)\cosh\xi_0(B\sin\eta - C\cos\eta)$$
$$- 2\lambda(\cosh 2\xi - \cosh 2\xi_0)(A\cosh\xi\sin\eta + C\sinh\xi\cos\eta)], \tag{27}$$

where

$$\frac{1}{\lambda} = 2\sinh\zeta\sinh\bar{\zeta} = \cosh 2\xi - \cos 2\eta \tag{28}$$

$$A = m - n\,e^{2\xi_0}\cos 2\beta \tag{29}$$

$$B = n\,e^{2\xi_0}\cos 2\beta \tag{30}$$

$$C = n\,e^{2\xi_0}\sin 2\beta. \tag{31}$$

One can verify that on the cavity one has $\sigma_\xi = \tau_{\xi\eta} = 0$. The first three equations are, in a more compact form, the stress tensor given by Chang and Wu [13]; the other two are new.

4. STRESSES AND DISPLACEMENTS AROUND AN ELLIPTICAL CAVITY

In the following we will depict the contour of principal stresses† defined by

$$\sigma_1 = \frac{\sigma_\xi + \sigma_\eta}{2} + \left[\left(\frac{\sigma_\xi - \sigma_\eta}{2}\right)^2 + \tau_{\xi\eta}^2\right]^{1/2} \tag{32}$$

$$\sigma_2 = \frac{\sigma_\xi + \sigma_\eta}{2} - \left[\left(\frac{\sigma_\xi - \sigma_\eta}{2}\right)^2 + \tau_{\xi\eta}^2\right]^{1/2} \tag{33}$$

$$\sigma_z = \nu(\sigma_\xi + \sigma_\eta) \quad \text{(plane strain)} \tag{34}$$

the von Mises criterion

$$\sigma_{eq}^2 = \tfrac{1}{2}[(\sigma_1 - \sigma_2)^2 + (\sigma_2 + \sigma_z)^2 + (\sigma_z - \sigma_1)^2] \tag{35}$$

the isochromatic lines

$$\tau_m = \tfrac{1}{2}(\sigma_1 - \sigma_2) \tag{36}$$

the isopachics for plane stress

$$\frac{2E}{\sigma v d}u_z = -\frac{\sigma_\xi - \sigma_\eta}{\sigma} = \text{const}, \tag{37}$$

where d is the plate thickness and E the Young modulus. Positive values (tractions if $\sigma > 0$) are full lines, negative values are dashed lines, and zero stresses are dashed–dotted lines.

Also depicted are the stress trajectories of principal stresses. In elliptical coordinates the slope of these stress trajectories is given by

$$m = \tan\alpha = \frac{\sigma_\eta - \sigma_\xi}{2\tau_{\xi\eta}} \pm \text{sign}(\tau_{\xi\eta})\left[\left(\frac{\sigma_\eta - \sigma_\xi}{2\tau_{\xi\eta}}\right)^2 + 1\right]^{1/2}, \tag{38}$$

where $\text{sign}(\tau_{\xi\eta})$ insures the continuity of the slope through the locus $\tau_{\xi\eta} = 0$. In the rectangular coordinate xOy, this slope is $\tan\gamma = dy/dx$. With

$$-\theta + \gamma - \alpha = \frac{\pi}{2},$$

where θ is the angle of the ellipse $\xi = c^{te}$ with the Ox axis:

$$\tan\theta = -\frac{\tanh\xi}{\tan\eta},$$

†Note that on the cavity $\sigma_1 = 0$ if $\sigma_\eta < 0$ and $\sigma_2 = 0$ if $\sigma_\eta > 0$. The point $\sigma_\eta = 0$ is marked by a small circle.

we obtain

$$\frac{dy}{dx} = \frac{m \tanh \xi + \tan \eta}{\tanh \xi - m \tan \eta}. \tag{39}$$

This differential equation is solved by the Runge–Kutta procedure. Also superimposed are the 0° and 45° isoclines related to the major axis of the ellipse and defined by $\tau_{xy} = 0$ or $\sigma_y - \sigma_x = 0$, i.e. from eqs (9) and (12)

$$2\tau_{xy} = -v(\sigma_y - \sigma_\xi) + 2u\tau_{\xi\eta} \tag{40}$$

$$\sigma_y - \sigma_x = u(\sigma_\eta - \sigma_\xi) + 2v\tau_{\xi\eta}, \tag{41}$$

where

$$u = \lambda(\cosh 2\xi \cos 2\eta - 1) \tag{42}$$

$$v = \lambda \sinh 2\xi \sin 2\eta. \tag{43}$$

Isotropic points ($\sigma_1 = \sigma_2$) are points where the slope of stress trajectories is not defined. They are marked by a small circle on the cavity ($\sigma_\eta = 0$), and can be found in the hinterland as points where 0° and 45° isoclines are crossing.

4.1. *Uniform loading*

When $k = 1$, ($n = 0; m = 2$), eqs (23)–(27) are greatly simplified:

$$\frac{\sigma_\xi}{\sigma} = \lambda^2 \sinh 2\xi(\cosh 2\xi - \cosh 2\xi_0) \tag{44}$$

$$\frac{\sigma_\eta}{\sigma} = \lambda \sinh 2\xi[2 - \lambda(\cosh 2\xi - \cosh 2\xi_0)] \tag{45}$$

$$\frac{\tau_{\xi\eta}}{\sigma} = \lambda^2 \sin 2\eta(\cosh 2\xi - \cosh 2\xi_0) \tag{46}$$

$$u_x = \frac{\sigma c}{4\mu}[\kappa + 1 - 2\lambda(\cosh 2\xi - \cosh 2\xi_0)]\sinh \xi \cos \eta \tag{47}$$

$$u_y = \frac{\sigma c}{4\mu}[\kappa + 1 - 2\lambda(\cosh 2\xi - \cosh 2\xi_0)]\cosh \xi \sin \eta. \tag{48}$$

The first three equations were given by Inglis [1]. On the cavity itself ($\xi = \xi_0$) we have $\sigma_\xi = \tau_{\xi\eta} = 0$ and

$$\frac{\sigma_\eta}{\sigma} = \frac{2 \sinh 2\xi_0}{\cosh 2\xi_0 - \cos 2\eta}, \tag{49}$$

which is maximum at the tip of the ellipse:

$$\sigma_y = (\sigma_\eta)_{\eta=0} = 2\frac{a}{b}\sigma. \tag{50}$$

On the x and y axes, the stresses can be written in Cartesian coordinates. On the x-axis ($\eta = 0$) where $\sigma_y \equiv \sigma_\eta$, $\sigma_x \equiv \sigma_\xi$ and $\tau_{xy} = 0$, we have

$$\left(\frac{\sigma_x}{\sigma}\right)_{y=0} = \frac{x(x^2 - a^2)}{(x^2 - a^2 + b^2)^{3/2}} \tag{51}$$

$$\left(\frac{\sigma_y}{\sigma}\right)_{y=0} = \frac{x}{(x^2 - a^2 + b^2)^{1/2}}\left(1 + \frac{b^2}{x^2 - a^2 - b^2}\right); \tag{52}$$

and on the y-axis ($\eta = \pi/2$), where $\sigma_y \equiv \sigma_\xi$ and $\sigma_x \equiv \sigma_\eta$, we have

$$\left(\frac{\sigma_x}{\sigma}\right)_{x=0} = \frac{y}{(y^2 + a^2 - b^2)^{1/2}}\left(1 + \frac{a^2}{y^2 + a^2 - b^2}\right) \tag{53}$$

$$\left(\frac{\sigma_y}{\sigma}\right)_{x=0} = \frac{y(y^2 - b^2)}{(y^2 + a^2 - b^2)^{3/2}}. \tag{54}$$

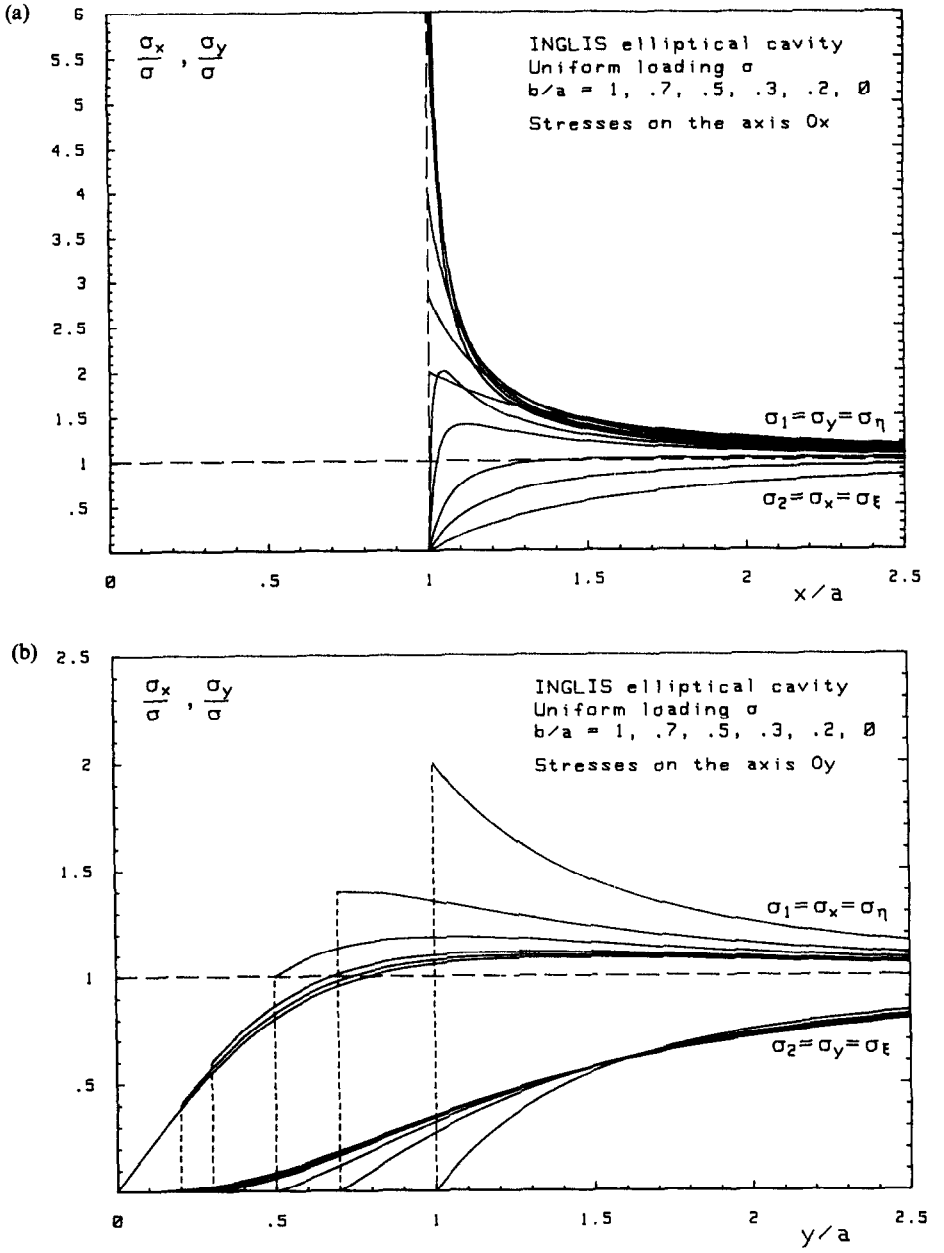

Fig. 2

These stresses are depicted in Fig. 2 for various b/a.

The displacements of the cavity points are simply

$$u_x = \frac{\sigma(\kappa+1)}{4\mu} b \cos\eta \tag{55}$$

$$u_y = \frac{\sigma(\kappa+1)}{4\mu} a \sin\eta. \tag{56}$$

Letting

$$S = \frac{\sigma(\kappa+1)}{8\mu}, \tag{57}$$

the new semi-axes of the deformed ellipse are

$$a' = a + 2bS \tag{58}$$

$$b' = b + 2aS. \tag{59}$$

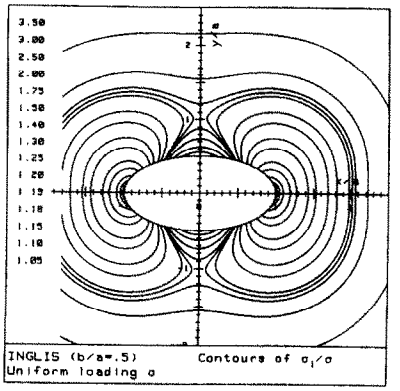
INGLIS (b/a=.5)
Uniform loading σ
Contours of σ1/σ

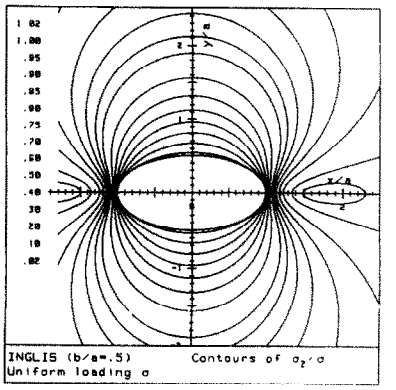
INGLIS (b/a=.5)
Uniform loading σ
Contours of σ2/σ

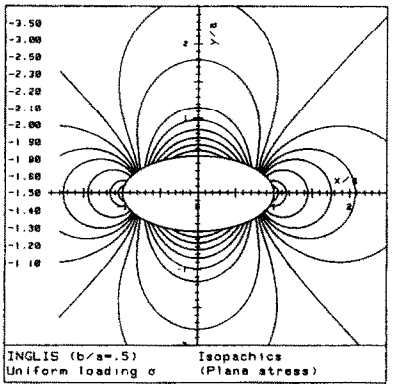
INGLIS (b/a=.5)
Uniform loading σ
Isopachics
(Plane stress)

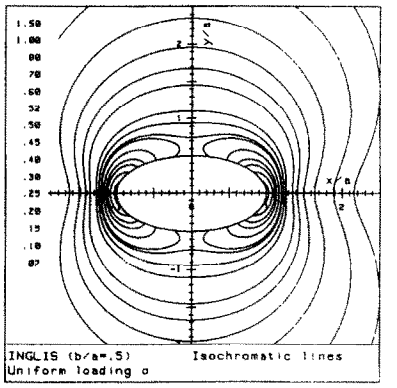
INGLIS (b/a=.5)
Uniform loading σ
Isochromatic lines

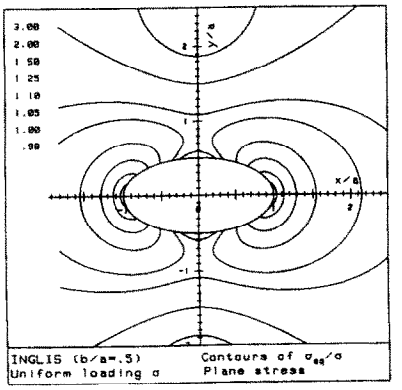
INGLIS (b/a=.5)
Uniform loading σ
Contours of σeq/σ
Plane stress

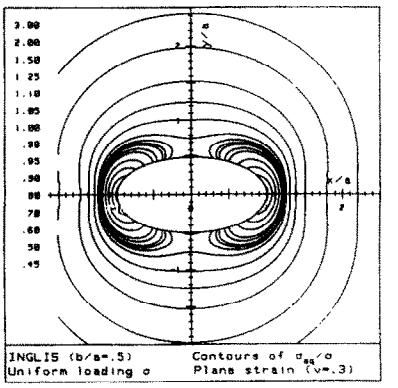
INGLIS (b/a=.5)
Uniform loading σ
Contours of σeq/σ
Plane strain (ν=.3)

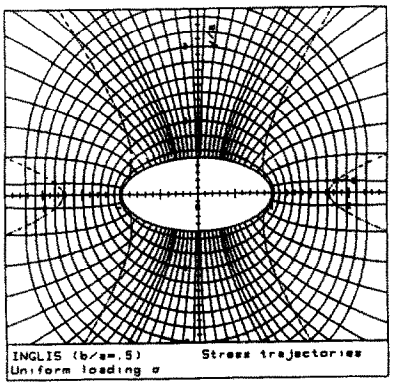
INGLIS (b/a=.5)
Uniform loading σ
Stress trajectories

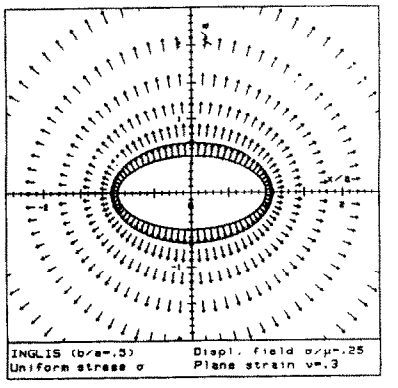
INGLIS (b/a=.5)
Uniform stress σ
Displ. field σ/μ=.25
Plane strain ν=.3

Fig. 3

Contours of principal stresses', von Mises criterion, isochromatic lines, isopachics, stress trajectories and the displacement field are given in Fig. 3 for $b/a = 1/2$. Such isochromatic lines were given by Küppers [14] for $b/a = 1/500$.

4.2. *Uniaxial loading with* $\beta = \pi/2$

In the case $k = 0$ ($m = n = 1, C = 0$), there is no major simplification. On the cavity itself we have

$$\left(\frac{\sigma_\eta}{\sigma}\right)_{\xi=\xi_0} = \frac{\sinh 2\xi_0 - 1 + e^{2\xi_0}\cos 2\eta}{\cosh 2\xi_0 - \cos 2\eta}, \tag{60}$$

which is maximum at the tip of the ellipse

$$\sigma_y = (\sigma_\eta)_{\eta=0} = \left(1 + 2\frac{a}{b}\right)\sigma \tag{61}$$

(results given by Inglis [1]), and zero for

$$\cos\eta = \left(1 + \frac{b}{a}\right)^{-1}. \tag{62}$$

At this latter point the two principal stresses are zero, and the slope of the stress trajectory is not defined (isotropic point).

On the x-axis ($\eta = 0$) we have

$$(a-b)^2\left(\frac{\sigma_x}{\sigma}\right)_{y=0} = -a^2 + \frac{a|x|}{(x^2 - a^2 + b^2)^{1/2}}\left[a - \frac{b^2(a-b)}{x^2 - a^2 + b^2}\right] \tag{63}$$

$$(a-b)^2\left(\frac{\sigma_y}{\sigma}\right)_{y=0} = b^2 + \frac{a|x|}{(x^2 - a^2 + b^2)^{1/2}}\left[a - 2b + \frac{b^2(a-b)}{x^2 - a^2 + b^2}\right] \tag{64}$$

and on the y-axis ($\eta = \pi/2$)

$$(a-b)^2\left(\frac{\sigma_x}{\sigma}\right)_{x=0} = -a^2 + \frac{a|y|}{(y^2 + a^2 - b^2)^{1/2}}\left[a + \frac{a^2(a-b)}{y^2 + a^2 - b^2}\right] \tag{65}$$

$$(a-b)^2\left(\frac{\sigma_y}{\sigma}\right)_{x=0} = b^2 + \frac{a|y|}{(y^2 + a^2 - b^2)^{1/2}}\left[a - 2b - \frac{a^2(a-b)}{y^2 + a^2 - b^2}\right]. \tag{66}$$

These stresses are depicted in Fig. 4 for various b/a, and are in agreement with the figure given by Inglis [1] for $a = 3b$. Note that at the end of the minor axis $\sigma_x = -\sigma$ instead of $(2b/a)\sigma$ for uniform loading.

The displacements of the cavity points are

$$u_x = -aS\cos\eta \tag{67}$$

$$u_y = (2a + b)S\sin\eta, \tag{68}$$

and the semi-axes of the deformed ellipse

$$a' = a(1 - S) \tag{69}$$

$$b' = b(1 + S) + 2aS. \tag{70}$$

The stress and displacement fields are given in Fig. 5. Note the existence on σ_1 and σ_2 of compressive stresses (for $\sigma > 0$) independent of the Poisson effect. [The Poisson ratio ν does not appear in the stress tensor; it only affects $\sigma_z = \nu(\sigma_1 + \sigma_2)$ in plane strain.] On the other hand, the Poisson effect clearly appears on the displacement field.

4.3. *The general case*

Let us study the inclined cavity under biaxial loading. On the cavity itself we have $\sigma_\xi = \tau_{\xi\eta} = 0$ and

$$\left(\frac{\sigma_\eta}{\sigma}\right)_{\xi=\xi_0} = B + \frac{A\sinh 2\xi_0 - C\sin 2\eta}{\cosh 2\xi_0 - \cos 2\eta}. \tag{71}$$

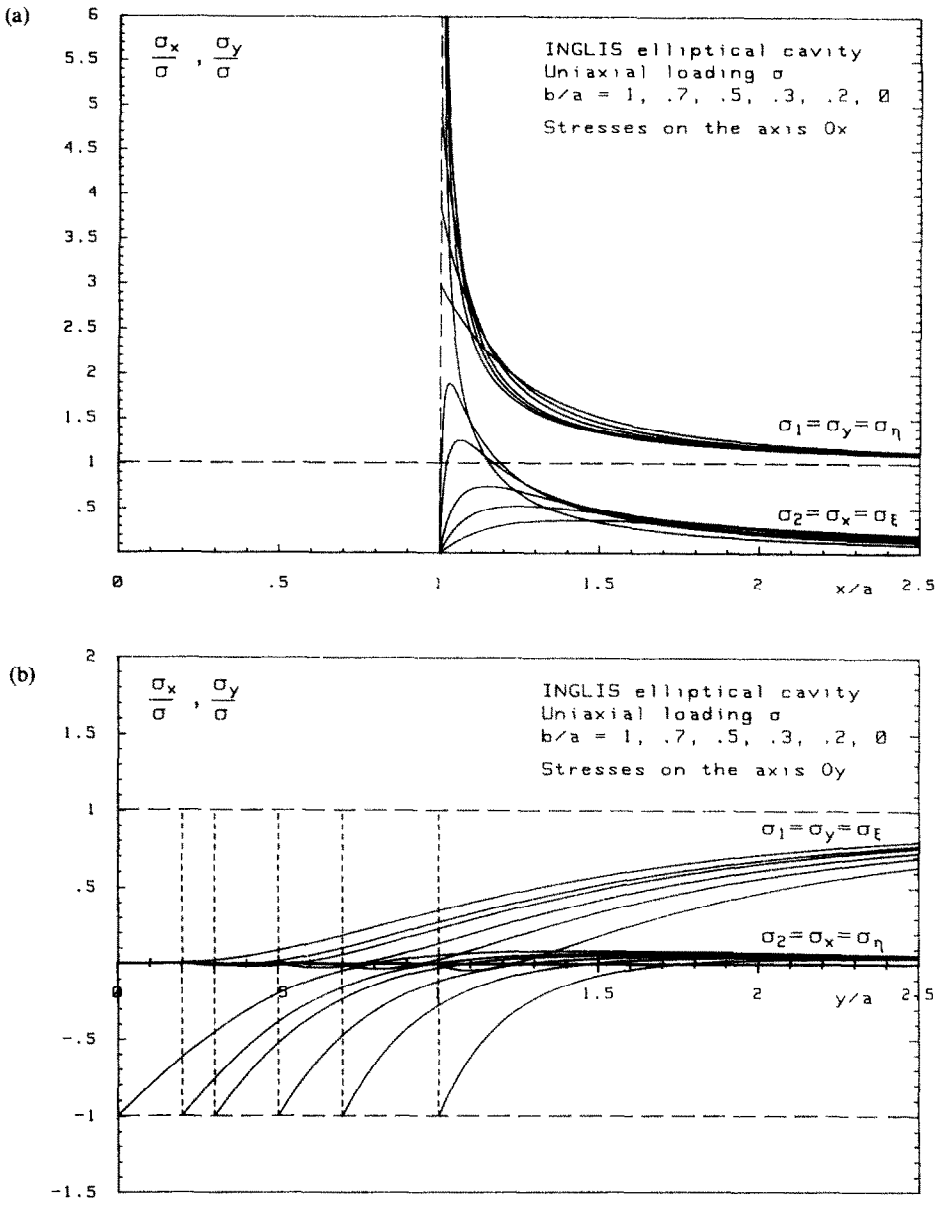

Fig. 4

On the minor axis ($\eta = \pi/2$) we have

$$\left(\frac{\sigma_\eta}{\sigma}\right)_{\xi=\xi_0} = \frac{\sigma_x}{\sigma} = n\cos 2\beta + (m + n\cos 2\beta)\frac{b}{a} \tag{72}$$

and on the major axis ($\eta = 0$)

$$\left(\frac{\sigma_\eta}{\sigma}\right)_{\xi=\xi_0} = \frac{\sigma_y}{\sigma} = -n\cos 2\beta + (m - n\cos 2\beta)\frac{a}{b} \tag{73}$$

with, for $\beta = \pi/2$,

$$\sigma_y = K_t\sigma = \left(n + \frac{2a}{b}\right)\sigma, \tag{73a}$$

where K_t is the stress concentration factor.

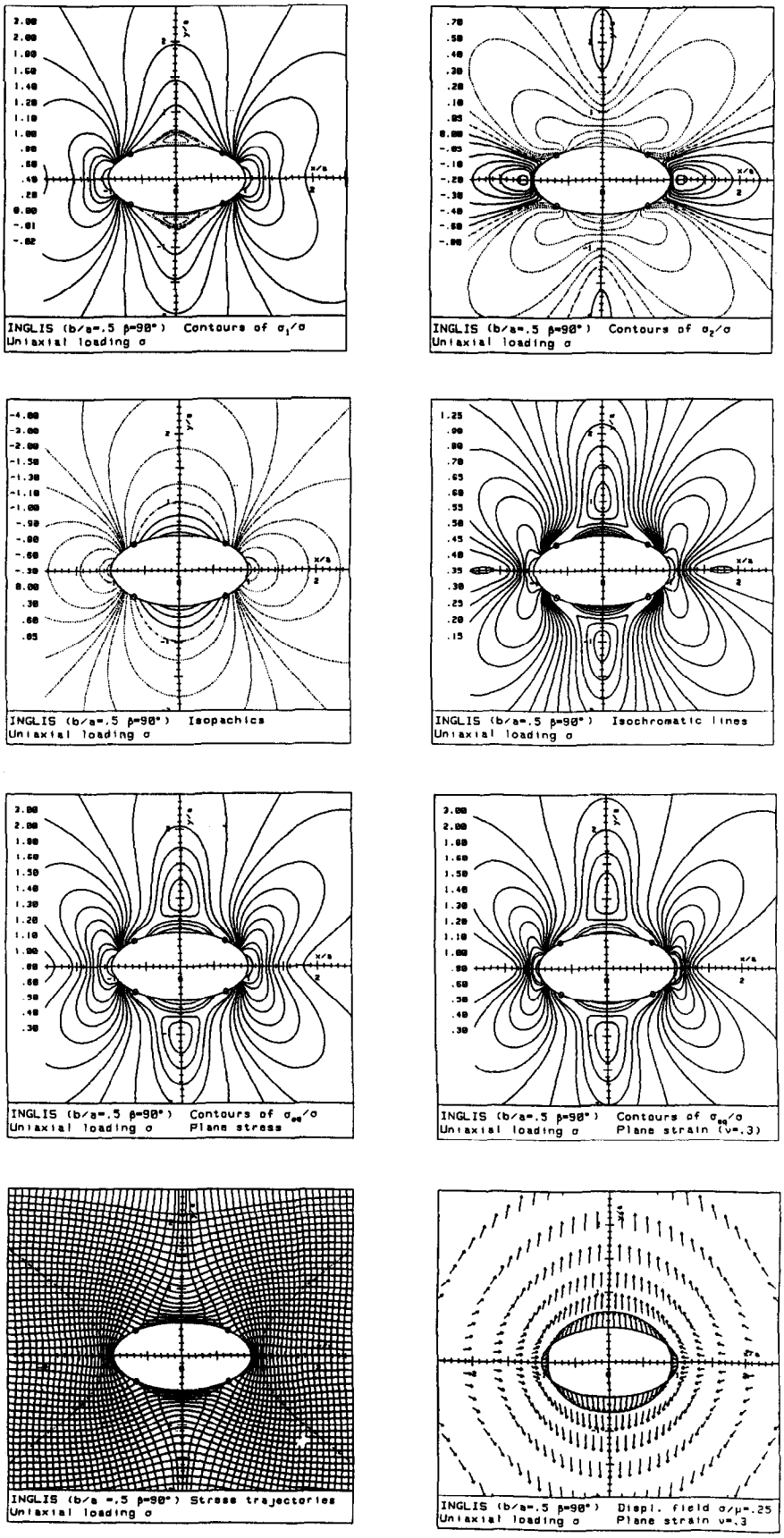
INGLIS (b/a=.5 β=90°) Contours of σ_1/σ
Uniaxial loading σ
INGLIS (b/a=.5 β=90°) Contours of σ_2/σ
Uniaxial loading σ
INGLIS (b/a=.5 β=90°) Isopachics
Uniaxial loading σ
INGLIS (b/a=.5 β=90°) Isochromatic lines
Uniaxial loading σ
INGLIS (b/a=.5 β=90°) Contours of σ_{ee}/σ
Uniaxial loading σ Plane stress
INGLIS (b/a=.5 β=90°) Contours of σ_{ee}/σ
Uniaxial loading σ Plane strain (ν=.3)
INGLIS (b/a =.5 β=90°) Stress trajectories
Uniaxial loading σ
INGLIS (b/a=.5 β=90°) Displ. field σ/μ=.25
Uniaxial loading σ Plane strain ν=.3

Fig. 5

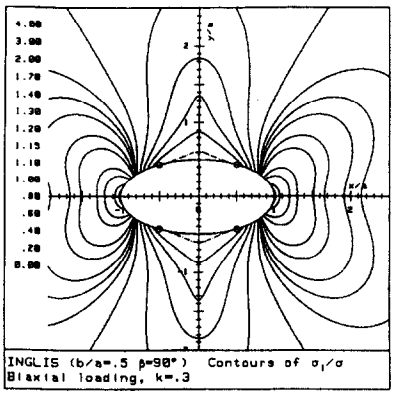
INGLIS (b/a=.5 β=90°) Contours of σ1/σ
Biaxial loading, k=.3

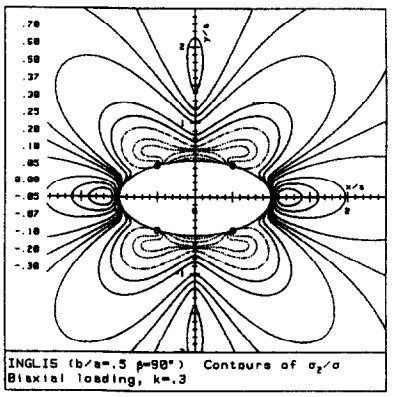
INGLIS (b/a=.5 β=90°) Contours of σ2/σ
Biaxial loading, k=.3

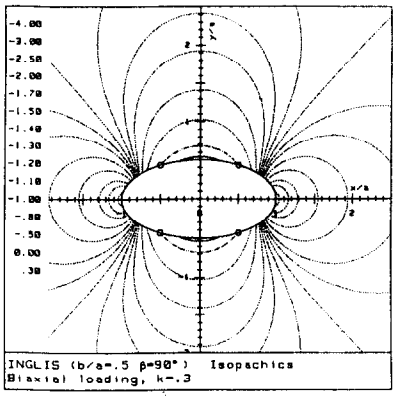
INGLIS (b/a=.5 β=90°) Isopachics
Biaxial loading, k=.3

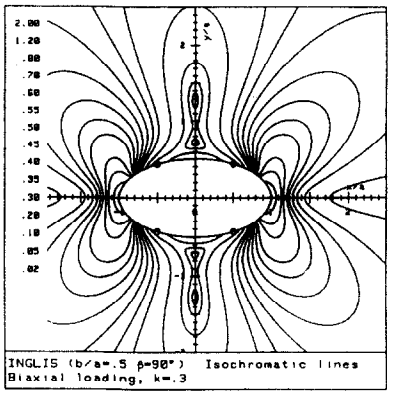
INGLIS (b/a=.5 β=90°) Isochromatic lines
Biaxial loading, k=.3

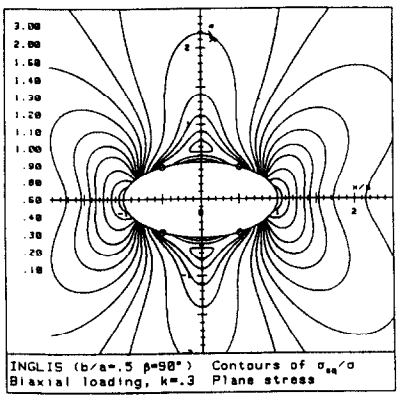
INGLIS (b/a=.5 β=90°) Contours of σeq/σ
Biaxial loading, k=.3 Plane stress

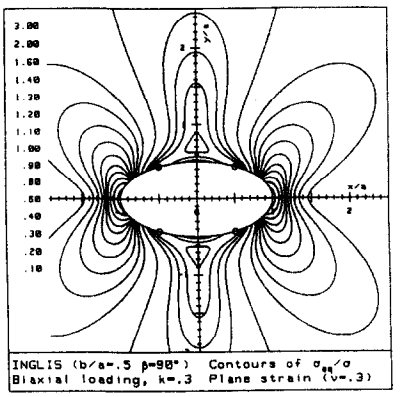
INGLIS (b/a=.5 β=90°) Contours of σeq/σ
Biaxial loading, k=.3 Plane strain (ν=.3)

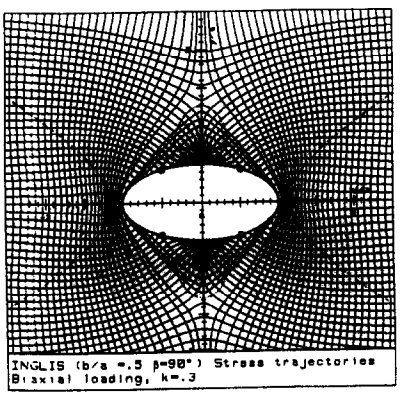
INGLIS (b/a =.5 β=90°) Stress trajectories
Biaxial loading, k=.3

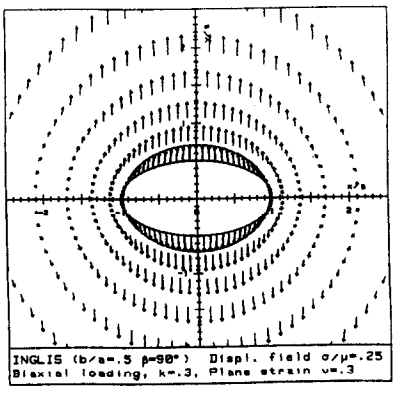
INGLIS (b/a=.5 β=90°) Displ. field σ/μ=.25
Biaxial loading, k=.3, Plane strain ν=.3

Fig. 6

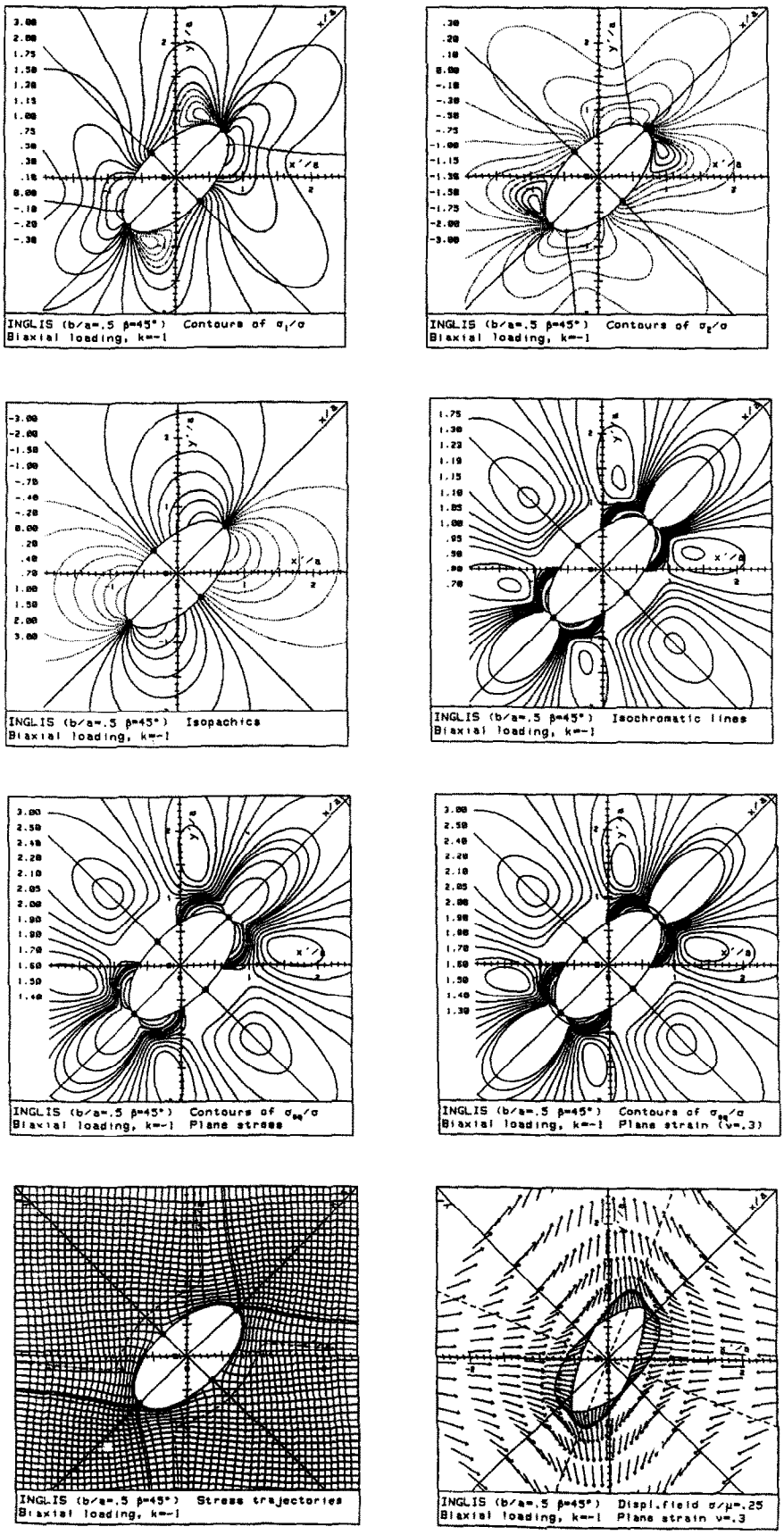
INGLIS (b/a=.5 β=45°) Contours of σ_1/σ
Biaxial loading, k=-1
INGLIS (b/a=.5 β=45°) Contours of σ_2/σ
Biaxial loading, k=-1
INGLIS (b/a=.5 β=45°) Isopachics
Biaxial loading, k=-1
INGLIS (b/a=.5 β=45°) Isochromatic lines
Biaxial loading, k=-1
INGLIS (b/a=.5 β=45°) Contours of σ_{xx}/σ
Biaxial loading, k=-1 Plane stress
INGLIS (b/a=.5 β=45°) Contours of σ_{xx}/σ
Biaxial loading, k=-1 Plane strain (ν=.3)
INGLIS (b/a=.5 β=45°) Stress trajectories
Biaxial loading, k=-1
INGLIS (b/a=.5 β=45°) Displ.field σ/μ=.25
Biaxial loading, k=-1 Plane strain ν=.3

Fig. 7

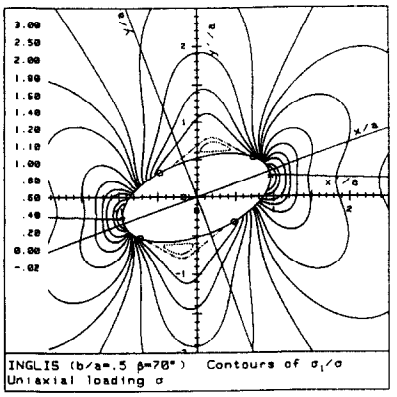
INGLIS (b/a=.5 β=70°) Contours of σ_1/σ
Uniaxial loading σ

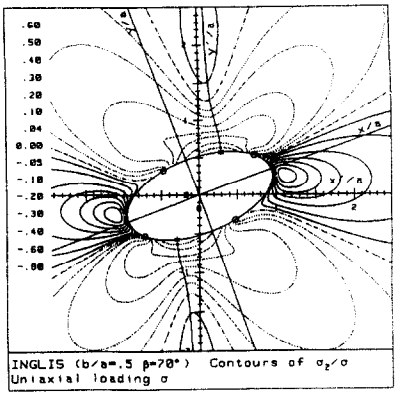
INGLIS (b/a=.5 β=70°) Contours of σ_2/σ
Uniaxial loading σ

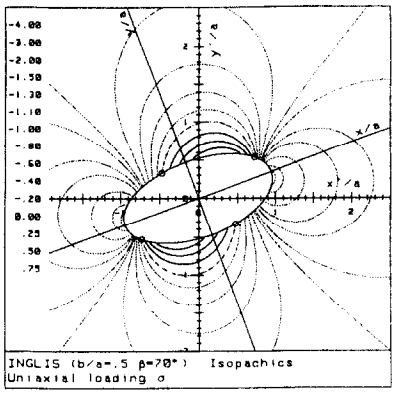
INGLIS (b/a=.5 β=70°) Isopachics
Uniaxial loading σ

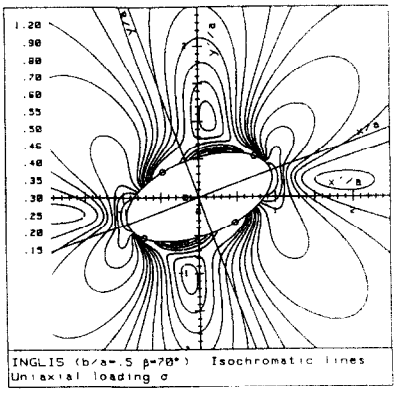
INGLIS (b/a=.5 β=70°) Isochromatic lines
Uniaxial loading σ

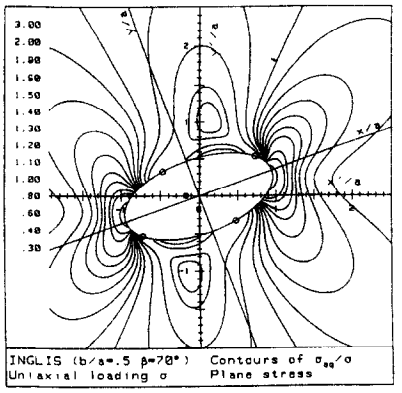
INGLIS (b/a=.5 β=70°) Contours of σ_{eq}/σ
Uniaxial loading σ Plane stress

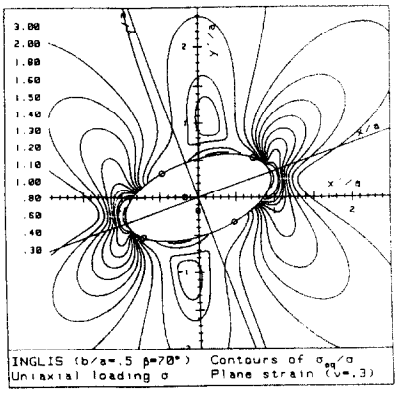
INGLIS (b/a=.5 β=70°) Contours of σ_{eq}/σ
Uniaxial loading σ Plane strain (ν=.3)

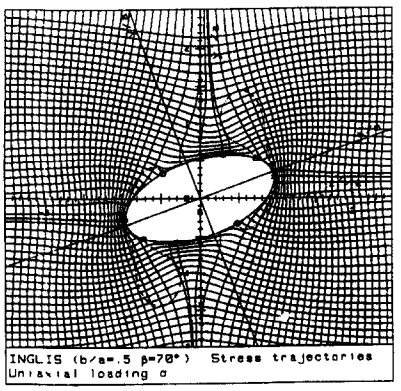
INGLIS (b/a=.5 β=70°) Stress trajectories
Uniaxial loading σ

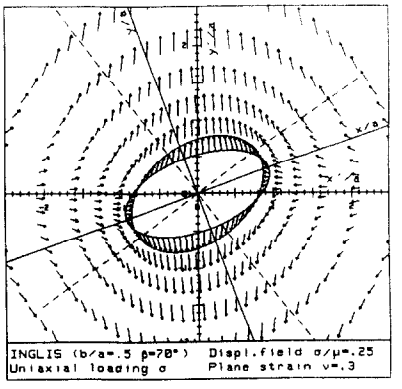
INGLIS (b/a=.5 β=70°) Displ.field σ/μ=.25
Uniaxial loading σ Plane strain ν=.3

Fig. 8

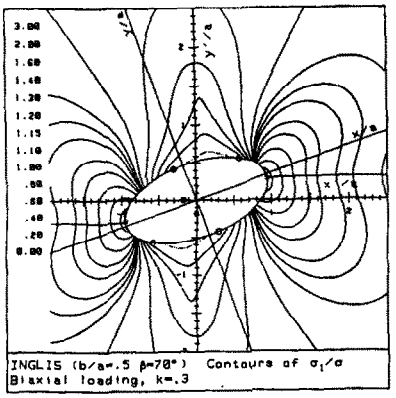
INGLIS (b/a=.5 β=70°) Contours of σ_1/σ
Biaxial loading, k=.3

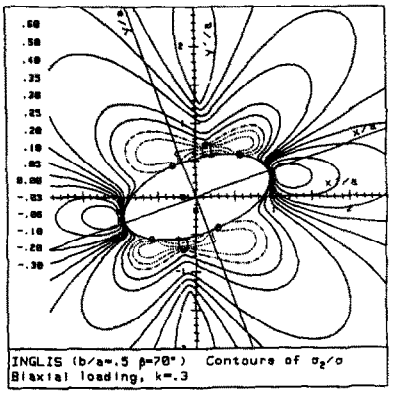
INGLIS (b/a=.5 β=70°) Contours of σ_2/σ
Biaxial loading, k=.3

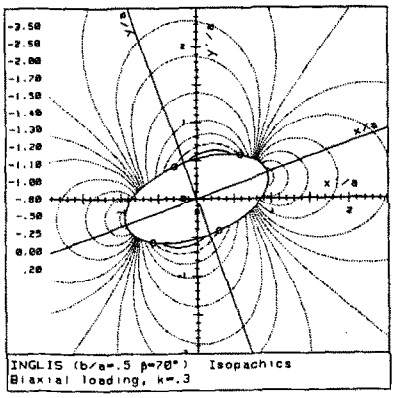
INGLIS (b/a=.5 β=70°) Isopachics
Biaxial loading, k=.3

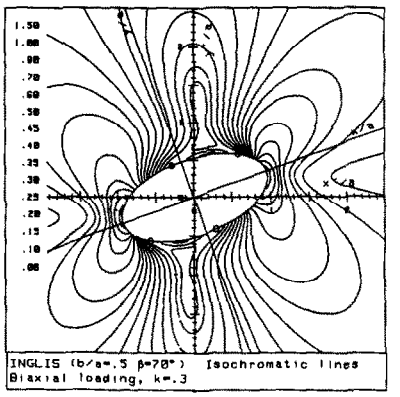
INGLIS (b/a=.5 β=70°) Isochromatic lines
Biaxial loading, k=.3

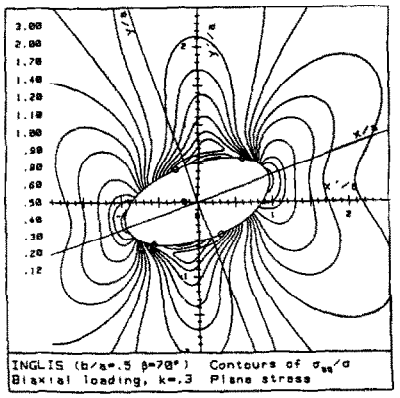
INGLIS (b/a=.5 β=70°) Contours of σ_{ss}/σ
Biaxial loading, k=.3 Plane stress

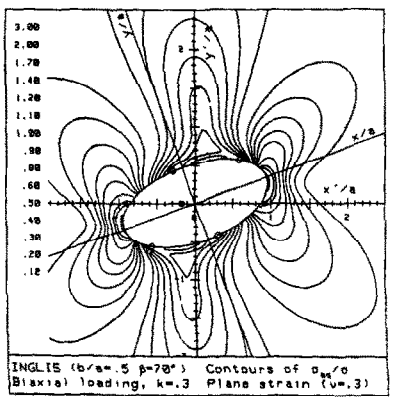
INGLIS (b/a=.5 β=70°) Contours of σ_{ss}/σ
Biaxial loading, k=.3 Plane strain (ν=.3)

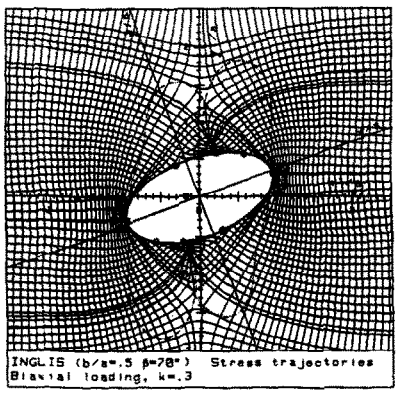
INGLIS (b/a=.5 β=70°) Stress trajectories
Biaxial loading, k=.3

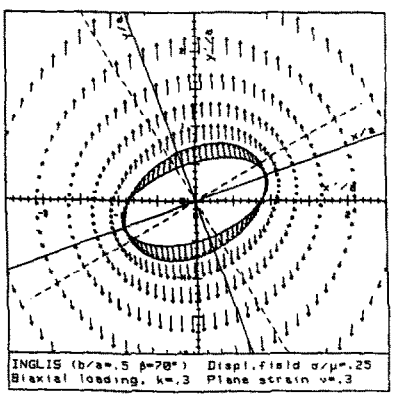
INGLIS (b/a=.5 β=70°) Displ.field σ/μ=.25
Biaxial loading, k=.3 Plane strain ν=.3

Fig. 9

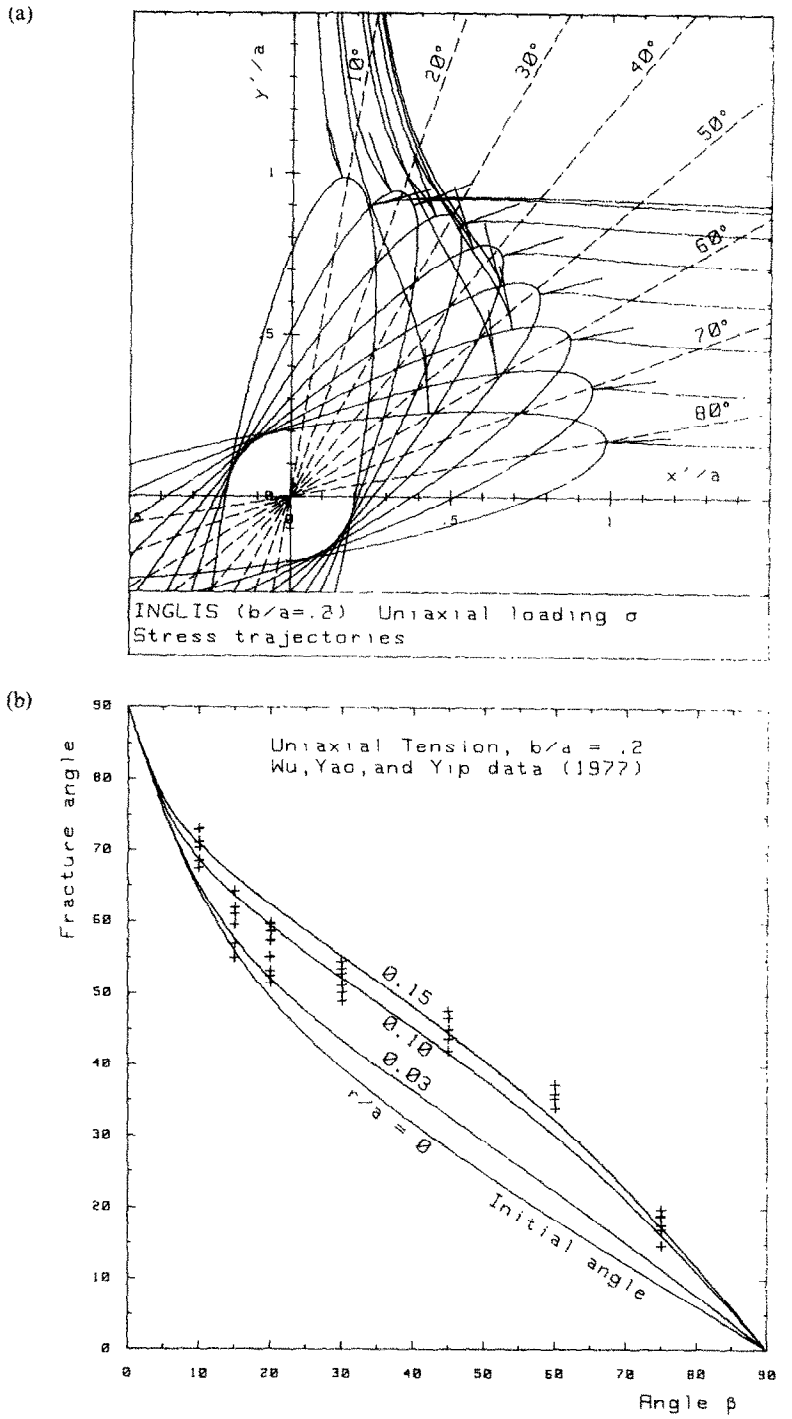

Fig. 10

The stress field and the displacement field are depicted in Figs 6–9 for various angles β and biaxiality factors k.

For $\beta \neq \pi/2$ we have drawn on σ_1 and σ_2 maps the stress trajectories starting from the more stressed points on the cavity, marked by an asterisk. If $\xi_0 \neq 0$ these points are defined by

$$\tan \eta = \frac{A \mp \sqrt{(A^2 + C^2)}}{C} \tanh \xi_0. \tag{74}$$

(The minus and plus signs refer, respectively, to the maximum and the minimum of σ_η/σ.) As the stress trajectories start perpendicular to the ellipse (slope $\tan\eta/\tanh\xi_0$), the initial slope of a stress trajectory starting from the more stressed point is

$$\tan\gamma = \frac{dy}{dx} = \frac{A \mp \sqrt{(A^2 + C^2)}}{C}. \tag{75}$$

It is generally accepted that a branched crack starts from the point of the highest tension [39] on the cavity and follows a stress trajectory [40] (propagation in mode I). In Figs 10a and 11a are shown these crack trajectories for $b/a = 0.1$ and 0.2 and for various angles β. The initial slope, eq.

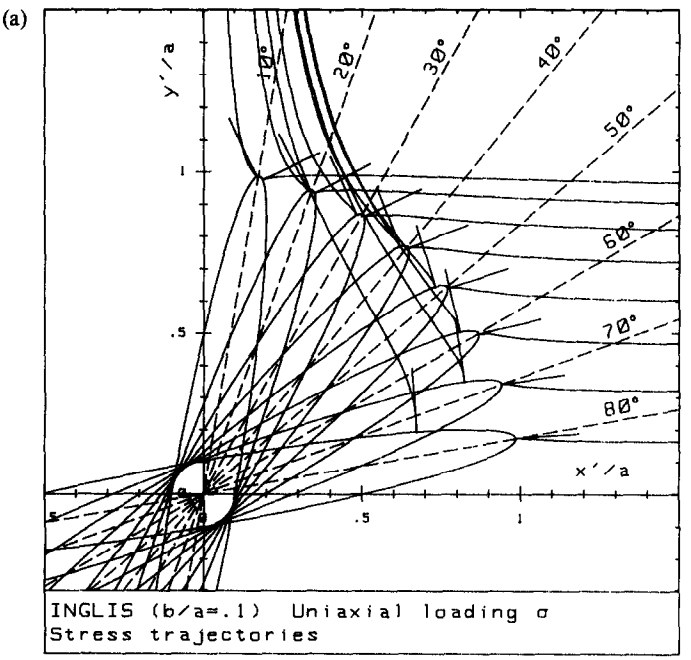

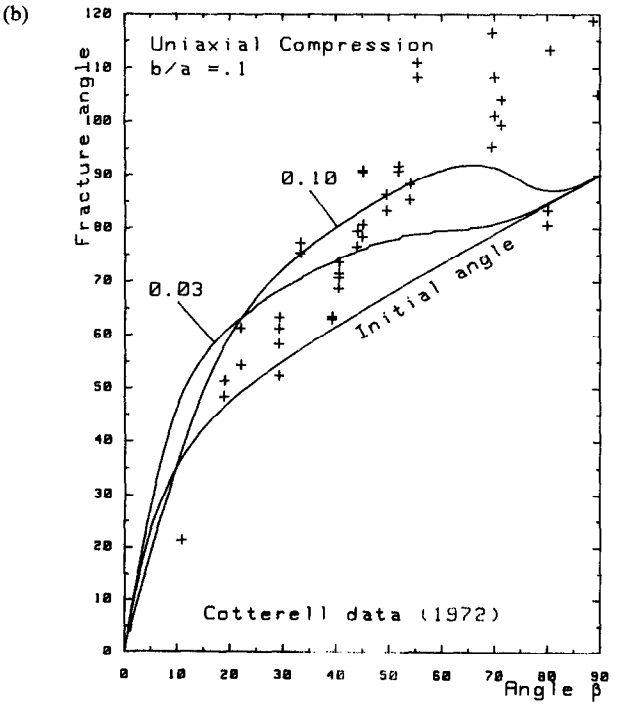

Fig. 11

(75), is given by a small segment, and the first point of the trajectory is taken on it at $r_0/a = 10^{-4}$ to avoid division by zero. One can see that the trajectory leaves the initial slope more rapidly as the ellipse is slender (as first observed by Cotterell [41]).

In Figs 10b and 11b, these results are compared to experimental data by Wu *et al.* [42] for uniaxial tension and by Cotterell [43] for uniaxial compression. As the trajectory is continuously turning, the fracture angles must have been measured at a distance r/a. The results are satisfactory for tension, but less satisfactory for compression. However, it must be emphasized that Cotterell [43] machined holes with a 400 grade silicon carbide powder, which left microcracks of about 20 μm. As observed and computed by Mouginot and Maugis [44] for Hertzian fracture, the crack does not start from the point where the tensile stress is maximum, but from the microcrack where the energy release rate is maximum at its tip. These curves are similar (although the r/a values are different) to those given by Chang [45] using the exact solution but computing the point at a distance r/a where the tangential stress is maximum (maximum tangential stress criterion). However, as pointed out by Maiti and Smith [46], the condition $\partial\sigma_\theta/\partial\theta = 0$ does not mean $\tau_{r\theta} = 0$, so that at this point σ_θ is not a principal stress. Maiti and Smith [46] used the maximum tangential principal stress (MTPS) criterion, looking where the principal stress is maximum on a circle of radius r/a centred on the point of the ellipse where σ_η is maximum. For uniaxial tension and $b/a = 0.2$, their results are identical to ours for $r/a = 0.001$, but can differ by 7° for $r/a = 0.10$, which means that the stress trajectory does not pass exactly on the maximum principal stress measured *on a circle*.

4.4. *Deformation of the cavity*

For $\xi = \xi_0$ the displacements are

$$u_x = Sc[(A \sinh \xi_0 + B \cosh \xi_0)\cos \eta + C(\cosh \xi_0 - \sinh \xi_0)\sin \eta] \tag{76}$$

$$u_y = Sc[(A \cosh \xi_0 + B \sinh \xi_0)\sin \eta + C(\cosh \xi_0 - \sinh \xi_0)\cos \eta)]. \tag{77}$$

After displacement, the points x and y of the cavity become $x_1 = x + u_x$, $y_1 = y + u_y$, i.e.

$$x_1/c = E \cos \eta + D \sin \eta \tag{78}$$

$$y_1/c = F \sin \eta + D \cos \eta \tag{79}$$

with

$$D = CS\, e^{-\xi_0} \tag{80}$$

$$E = AS \sinh \xi_0 + (BS + 1)\cosh \xi_0 \tag{81}$$

$$F = AS \cosh \xi_0 + (BS + 1)\sinh \xi_0. \tag{82}$$

By eliminating $\sin \eta$ and $\cos \eta$ in eqs (78) and (79) we obtain the quadratic equation

$$(D^2 + F^2)x_1^2 + (D^2 + E^2)y_1^2 - 2D(E + F)x_1 y_1 - c^2(EF - D^2)^2 = 0, \tag{83}$$

which represents an ellipse. To eliminate the crossed terms, let us change the variables:

$$x_1 = X \cos \alpha - Y \sin \alpha$$

$$y_1 = X \sin \alpha + Y \cos \alpha.$$

The XY terms disappear for

$$\tan 2\alpha = \frac{2D}{E - F} \tag{84}$$

and eq. (83) can be written

$$\frac{X'^2}{a'^2} + \frac{Y'^2}{b'^2} = 1 \tag{85}$$

with

$$\frac{a'^2}{c^2} = \frac{(EF - D^2)^2}{(F^2 - E^2)\cos^2 \alpha - 2D(E + F)\sin \alpha \cos \alpha + D^2 + E^2} = \tfrac{1}{4}(E + F - \sqrt{H})^2 \tag{86}$$

$$\frac{b^2}{c^2}=\frac{(EF-D^2)^2}{(E^2-F^2)\cos^2\alpha+2D(E-F)\sin\alpha\cos\alpha+D^2+F^2}=\tfrac{1}{4}(E+F-\sqrt{H})^2 \tag{87}$$

and

$$\begin{aligned}H&=4D^2+(E-F)^2\geqslant 0\\&=(E+F)^2+4(D^2-EF)\\&=(1-mS)^2\,e^{-2\xi_0}+4nS(1-mS)\cos 2\beta+4n^2S^2\,e^{2\xi_0}.\end{aligned} \tag{88}$$

Finally, we have

$$a'=\frac{c}{2}|E+F+\sqrt{H}| \tag{89}$$

$$b'=\frac{c}{2}|E+F-\sqrt{H}| \tag{90}$$

with

$$E+F=(1+mS)e^{\xi_0}. \tag{91}$$

One can verify that $a'=a$ and $b'=b$ when $S=0$.

When $D^2-EF\to 0$, one of the two semi-axes becomes zero, and it can easily be shown that $EF-D^2<0$ corresponds to interpenetration of matter. So, the condition of non-interpenetration would be

$$S^2[m^2\sinh 2\xi_0+2n(m\cos 2\beta-n\,e^{2\xi_0})]+2S(m\cosh 2\xi_0-n\cos 2\beta)+\sinh 2\xi_0\geqslant 0. \tag{92}$$

However, these results have been obtained in the frame of linearized elasticity, so that second order terms must be dropped out. Neglecting the S^2 terms we finally have

$$a'=a(1+Sn\cos 2\beta)+bS(m+n\cos 2\beta) \tag{93}$$

$$b'=b(1-Sn\cos 2\beta)+aS(m-n\cos 2\beta) \tag{94}$$

$$\sin 2\alpha=2Sn\,e^{2\xi_0}\sin 2\beta. \tag{95}$$

5. STRESSES AND DISPLACEMENTS AROUND CRACKS

There are no mathematical problems to make $b=0$ (i.e. $\xi_0=0$) in eqs (23)–(27), and the result in elliptical coordinates is

$$\frac{\sigma_\eta+\sigma_\xi}{\sigma}=n\cos 2\beta+\lambda[(m-n\cos 2\beta)\sinh 2\xi-n\sin 2\beta\sin 2\eta] \tag{96}$$

$$\begin{aligned}\frac{\sigma_\eta-\sigma_\xi}{\sigma}&=\lambda^2(m-n\cos 2\beta)\sinh 2\xi(1-\cos 2\eta)\\&\quad-\lambda n\cos 2\beta(\cosh 2\xi\cos 2\eta-1)-\lambda n\sin 2\beta[\cosh 2\xi-\lambda(\cosh 2\xi-1)]\sin 2\eta\end{aligned} \tag{97}$$

$$\begin{aligned}\frac{2\tau_{\xi\eta}}{\sigma}&=\lambda^2(m-n\cos 2\beta)(\cosh 2\xi-1)\sin 2\eta\\&\quad-\lambda n\cos 2\beta\sinh 2\xi\sin 2\eta+\lambda n\sin 2\beta\sinh 2\xi[\cos 2\eta-\lambda(1-\cos 2\eta)]\end{aligned} \tag{98}$$

$$\begin{aligned}u_x=\frac{\sigma a}{8\mu}\Big\{&(\kappa+1)\Big(\frac{x}{a}n\cos 2\beta-\frac{y}{a}n\sin 2\beta\Big)+(m-n\cos 2\beta)[\kappa+1-2\lambda(\cosh 2\xi-1)]\\&\times\sinh\xi\cos\eta+n\sin 2\beta[\kappa+1+2\lambda(\cosh 2\xi-1)]\cosh\xi\sin\eta\Big\}\end{aligned} \tag{99}$$

$$\begin{aligned}u_y=\frac{\sigma a}{8\mu}\Big\{&(\kappa-3)\frac{y}{a}n\cos 2\beta+(\kappa+1)\frac{x}{a}n\sin 2\beta+(m-n\cos 2\beta)[\kappa+1-2\lambda(\cosh 2\xi-1)]\\&\times\cosh\xi\sin\eta-n\sin 2\beta[\kappa-3+2\lambda(\cosh 2\xi-1)]\sinh\xi\cos\eta\Big\}.\end{aligned} \tag{100}$$

Using eqs (40)–(43) to change the coordinate, and eqs (A1)–(A12), we have in Cartesian coordinates

$$\frac{\sigma_y+\sigma_x}{\sigma} = n\cos 2\beta + \frac{R}{2}(m - n\cos 2\beta) - \frac{T}{2}n\sin 2\beta \tag{101}$$

$$\frac{\sigma_y-\sigma_x}{\sigma} = -n\cos 2\beta + P(m - n\cos 2\beta) + \left(\frac{T}{2}+Q\right)n\sin 2\beta \tag{102}$$

$$\frac{2\tau_{xy}}{\sigma} = Q(m - n\cos 2\beta) + \left(\frac{R}{2}-P\right)n\sin 2\beta \tag{103}$$

$$u_x = \frac{\sigma a}{8\mu}\left\{(\kappa+1)(Xn\cos 2\beta - Yn\sin 2\beta) + (m - n\cos 2\beta)\left[\kappa - \frac{X^2+Y^2-1}{\sqrt{\Delta}}\right]V + n\sin 2\beta\left[\kappa + 2 + \frac{X^2+Y^2-1}{\sqrt{\Delta}}\right]U\right\} \tag{104}$$

$$u_y = \frac{\sigma a}{8\mu}\left\{(\kappa-3)Yn\cos 2\beta + (\kappa+1)Xn\sin 2\beta + (m - n\cos 2\beta)\left[\kappa - \frac{X^2+Y^2-1}{\sqrt{\Delta}}\right]U - n\sin 2\beta\left[\kappa - 2 + \frac{X^2+Y^2-1}{\sqrt{\Delta}}\right]V\right\}, \tag{105}$$

where

$$R \equiv 2\lambda\sinh 2\xi = \left[\frac{(X^2+Y^2+\sqrt{\Delta})^2-1}{\Delta}\right]^{1/2} \tag{106}$$

$$T \equiv 2\lambda\sin 2\eta = \mathrm{sign}(xy)\left[\frac{1-(X^2+Y^2-\sqrt{\Delta})^2}{\Delta}\right]^{1/2} \tag{107}$$

$$P \equiv \lambda^2\sinh 2\xi(1-\cos 2\eta)[2\lambda(\cosh 2\xi\cos 2\eta - 1)+1] = \frac{YU}{\Delta^{3/2}}[2(X^2-Y^2-1)+\sqrt{\Delta}] \tag{108}$$

$$Q \equiv \lambda^2\sin 2\eta(\cosh 2\xi - 1)[2\lambda(\cosh 2\xi\cos 2\eta - 1)-1] = \frac{YV}{\Delta^{3/2}}[2(X^2-Y^2-1)+\sqrt{\Delta}]. \tag{109}$$

Note that on the X-axis $P = Q = 0$ and if $|X| > 1$

$$U = T = 0$$

$$V = \mathrm{sign}(X)\sqrt{(X^2-1)}$$

$$R = \frac{2|X|}{\sqrt{(X^2-1)}}$$

if $|X| < 1$

$$V = R = 0$$

$$U = \pm\sqrt{(1-X^2)}$$

$$T = \frac{2|X|}{\sqrt{(1-X^2)}}.$$

Note also that for $k = 0$ (uniaxial) and $\beta = 0°$, one has everywhere $\sigma_x = \sigma$ and $\sigma_y = \tau_{xy} = 0$ as if the crack did not exist.

Expressions are particularly simple for mode I ($\beta = 90°$). In this case we have

$$\frac{\tau_m}{\sigma} = \left[n\left(\frac{n}{4}+P\right)+\frac{Y^2}{\Delta^{3/2}}\right]^{1/2} \qquad \text{isochromatic lines} \tag{110}$$

$$\frac{\sigma_1}{\sigma} = \frac{R-n}{2} + \frac{\tau_m}{\sigma} \tag{111}$$

$$\frac{\sigma_2}{\sigma} = \frac{R-n}{2} - \frac{\tau_m}{\sigma} \tag{112}$$

$$\frac{\sigma_z}{\sigma} = \nu(R-n) \qquad \text{for plane strain} \qquad (113)$$

$$\frac{2E}{\nu\sigma d}u_z = -(R-n) \qquad \text{isopachics (plane stress)} \qquad (114)$$

$$\frac{\sigma_{eq}^2}{\sigma^2} = 3\left(\frac{\tau_m}{\sigma}\right)^2 + \left(\frac{R-n}{2}\right)^2 \qquad \text{plane stress} \qquad (115)$$

$$\frac{\sigma_{eq}^2}{\sigma^2} = 3\left(\frac{\tau_m}{\sigma}\right)^2 + (1-2\nu)^2\left(\frac{R-n}{2}\right)^2 \qquad \text{plane strain} \qquad (116)$$

$$\frac{dY}{dX} = \frac{n+2P}{2Q} \pm \text{sign}(Q)\left[\left(\frac{n+2P}{2Q}\right)^2 + 1\right]^{1/2} \qquad \text{stress trajectories.} \qquad (117)$$

Figures 12–14 show stresses and displacements for mode I. The isochromatic lines in Fig. 12 for uniform loading were given for the first time by Sneddon [15] in 1946, and those in Fig. 13 for uniaxial loading by Rothman and Ross [47]. Figures 13 are also in agreement with those given by Dixon [48, 49]. Note that in uniaxial loading the crack lips undergo a compressive stress $\sigma_x = -\sigma$ (see also Fig. 4). For thin sheets, this compression leads to buckling: the cracks have an out of plane motion either both in the same direction, or in opposite directions as observed by Dixon and Strannigan [49]. More precisely, as shown in Fig. 13, the whole plate undergoes compressive stress σ_2 at an angle of 45° to the fissure. As observed by Gilabert *et al.* [50], this compression provokes quasi-periodic buckling deformations aligned along σ_2 stress trajectories, in a pattern resembling a Maltese cross. This buckling due to the σ_2 stresses was also observed by Theocaris *et al.* [37] on rubber sheets.

In mode II also ($\beta = 45°, k = -1$), expressions can be simplified by noting that

$$\frac{\tau_m^2}{\sigma^2} = \frac{Y^2}{\Delta^{3/2}}(3 - 6X^2 - 2Y^2) + \frac{X^2+Y^2}{\sqrt{\Delta}}, \qquad (118)$$

directly giving the isochromatic lines. Stresses and displacements are shown in Fig. 15.

Returning to the *general case* (see Figs 16 and 17 for $\beta = 70°$), stresses and displacement have simple forms on the x and y axes.

On the x-axis (the crack axis) and for $|x| > a$, one has

$$(\sigma_y)_{y=0} = \frac{\sigma}{2}(m - n\cos 2\beta)\frac{|x|}{(x^2-a^2)^{1/2}} \qquad (119)$$

$$(\sigma_x)_{y=0} = \sigma_y + \sigma n \cos 2\beta \qquad (120)$$

$$(\tau_{xy})_{y=0} = \frac{\sigma}{2} n \sin 2\beta \frac{|x|}{(x^2-a^2)^{1/2}} \qquad (121)$$

$$(u_x)_{y=0} = \text{sign}(x)\frac{\sigma}{8\mu}[n\cos 2\beta(\kappa+1)|x| + (m - n\cos 2\beta)(\kappa-1)\sqrt{(x^2-a^2)}] \qquad (122)$$

$$(u_y)_{y=0} = \text{sign}(x)\frac{\sigma}{8\mu} n \sin 2\beta[(\kappa+1)|x| - (\kappa-1)\sqrt{(x^2-a^2)}] \qquad (123)$$

and for $|x| < a$ (the crack lips) one has

$$\sigma_y = \tau_{xy} = 0$$

$$(\sigma_x)_{y=0} = \sigma n\left(\cos 2\beta - \frac{|x|}{\sqrt{(a^2-x^2)}\sin 2\beta}\right) \qquad (124)$$

$$(u_x)_{y=0} = \frac{\sigma}{8\mu}(\kappa+1)[xn\cos 2\beta \pm n\sin 2\beta\sqrt{(a^2-x^2)}] \qquad (125)$$

$$(u_y)_{y=0} = \frac{\sigma}{8\mu}(\kappa+1)[xn\sin 2\beta \pm (m - n\cos 2\beta)\sqrt{(a^2-x^2)}] \qquad (126)$$

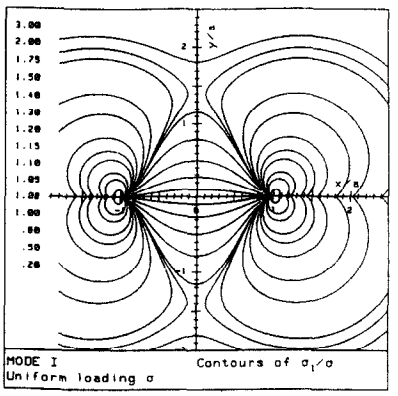
MODE I
Uniform loading σ
Contours of σ1/σ

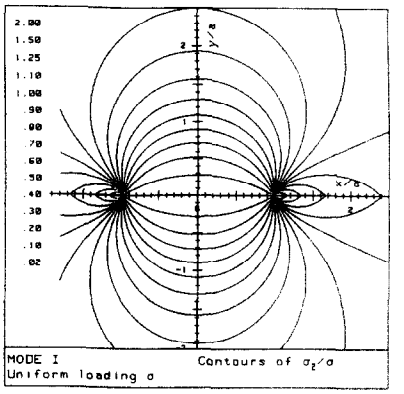
MODE I
Uniform loading σ
Contours of σ2/σ

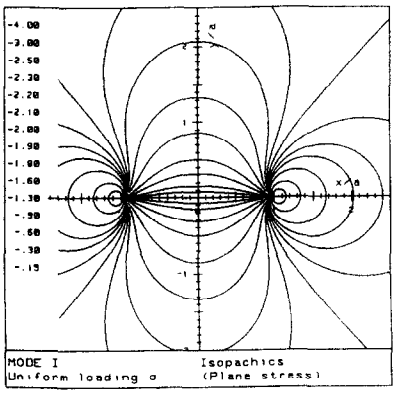
MODE I
Uniform loading σ
Isopachics
(Plane stress)

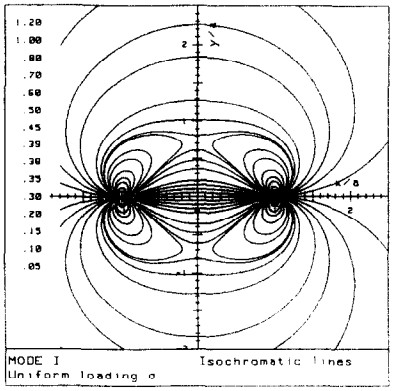
MODE I
Uniform loading σ
Isochromatic lines

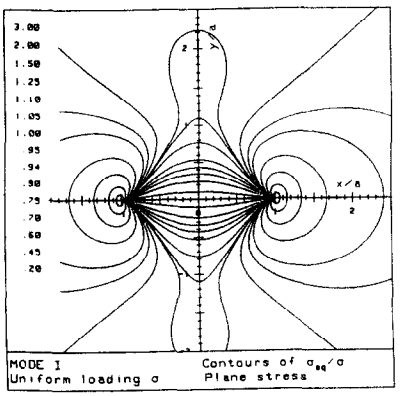
MODE I
Uniform loading σ
Contours of σeq/σ
Plane stress

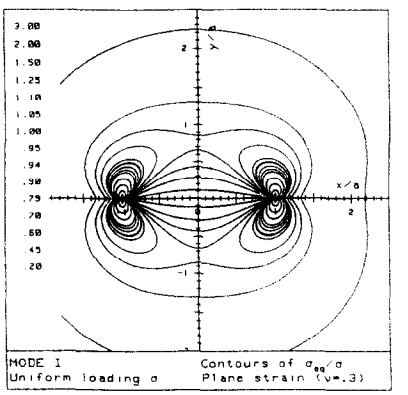
MODE I
Uniform loading σ
Contours of σeq/σ
Plane strain (ν=.3)

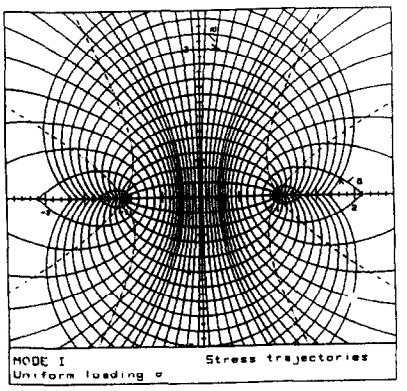
MODE I
Uniform loading σ
Stress trajectories

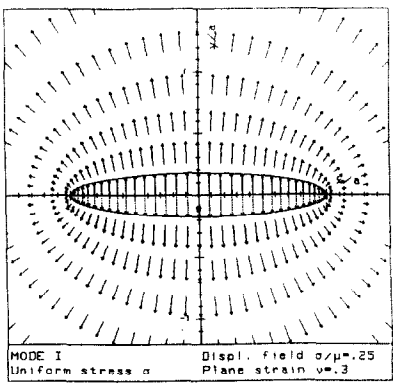
MODE I
Uniform stress σ
Displ. field σ/μ=.25
Plane strain ν=.3

Fig. 12

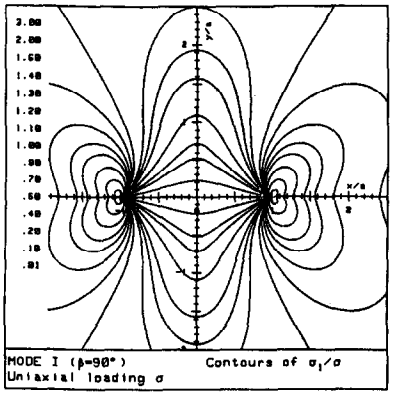
MODE I (β=90°)
Uniaxial loading σ
Contours of σ1/σ

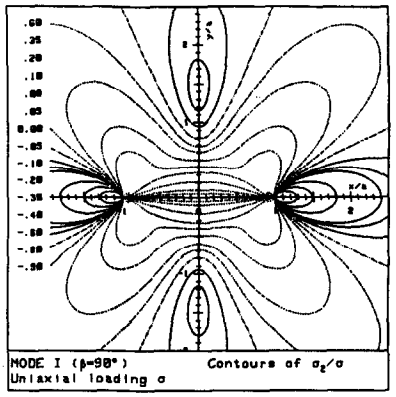
MODE I (β=90°)
Uniaxial loading σ
Contours of σ2/σ

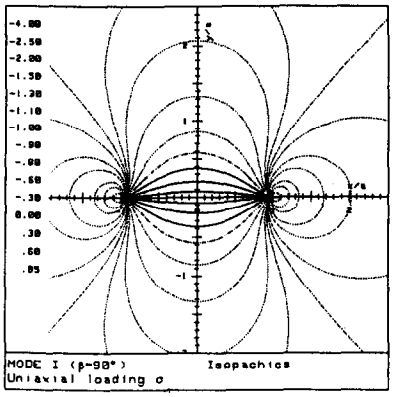
MODE I (β=90°)
Uniaxial loading σ
Isopachics

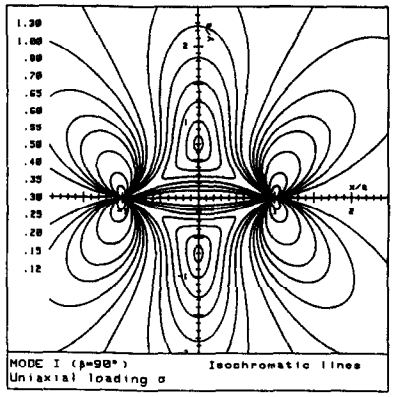
MODE I (β=90°)
Uniaxial loading σ
Isochromatic lines

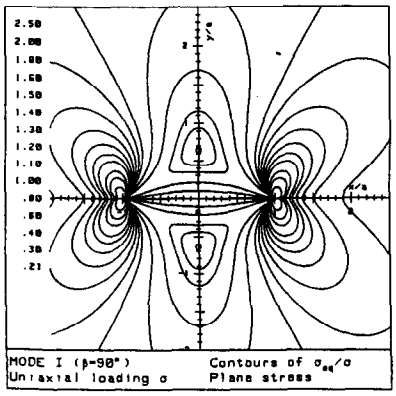
MODE I (β=90°)
Uniaxial loading σ
Contours of σeq/σ
Plane stress

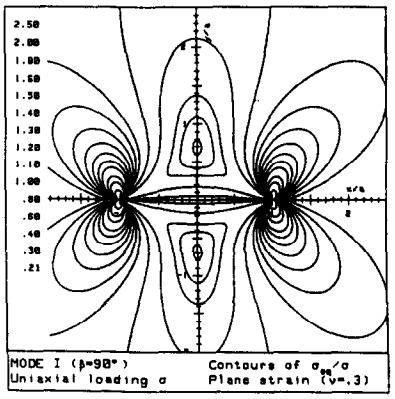
MODE I (β=90°)
Uniaxial loading σ
Contours of σeq/σ
Plane strain (ν=.3)

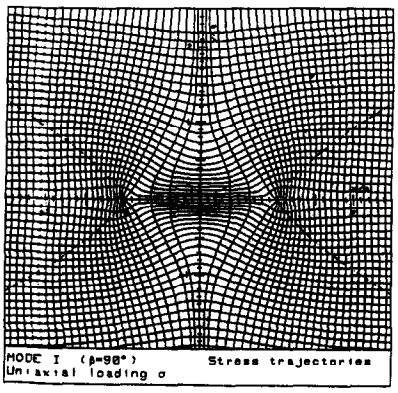
MODE I (β=90°)
Uniaxial loading σ
Stress trajectories

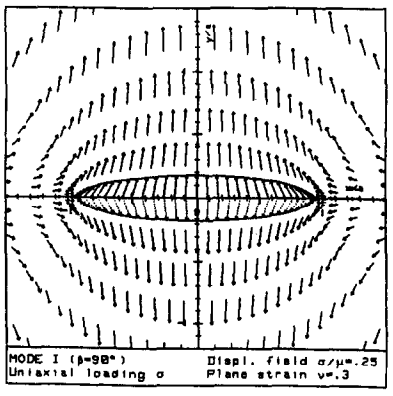
MODE I (β=90°)
Uniaxial loading σ
Displ. field σ/μ=.25
Plane strain ν=.3

Fig. 13

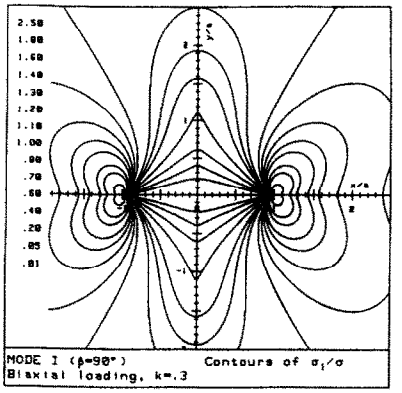
MODE I (β=90°) Contours of σ_1/σ
Biaxial loading, k=.3

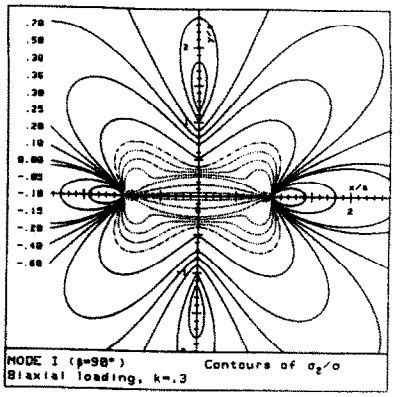
MODE I (β=90°) Contours of σ_2/σ
Biaxial loading, k=.3

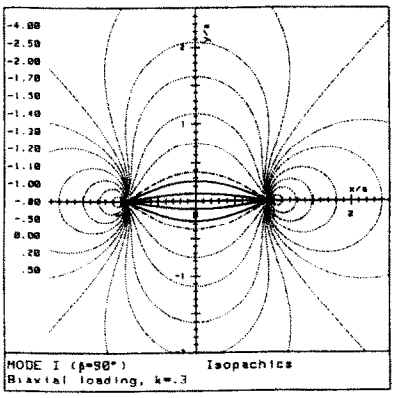
MODE I (β=90°) Isopachics
Biaxial loading, k=.3

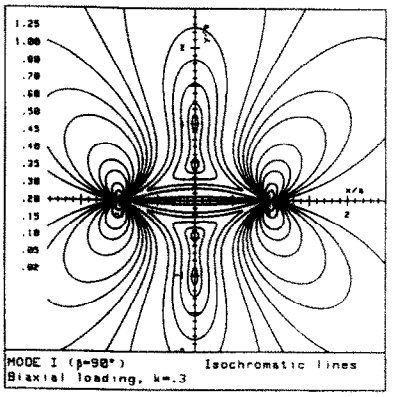
MODE I (β=90°) Isochromatic lines
Biaxial loading, k=.3

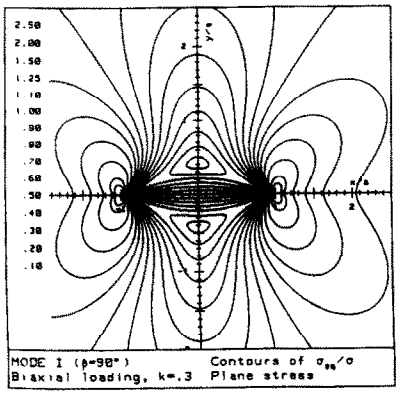
MODE I (β=90°) Contours of σ_{zz}/σ
Biaxial loading, k=.3 Plane stress

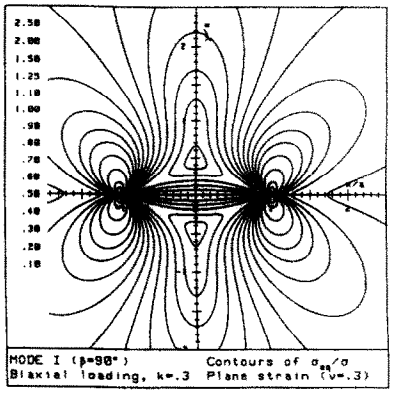
MODE I (β=90°) Contours of σ_{zz}/σ
Biaxial loading, k=.3 Plane strain (ν=.3)

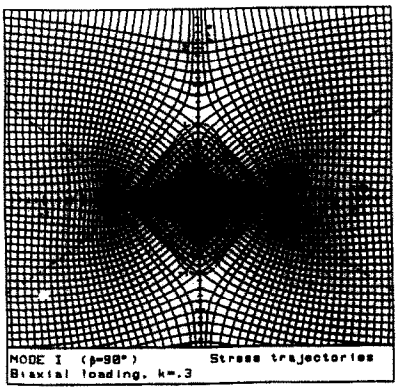
MODE I (β=90°) Stress trajectories
Biaxial loading, k=.3

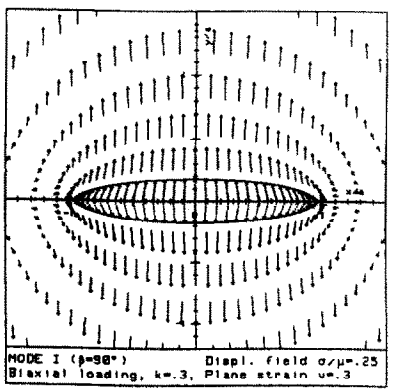
MODE I (β=90°) Displ. field σ/μ=.25
Biaxial loading, k=.3, Plane strain ν=.3

Fig. 14

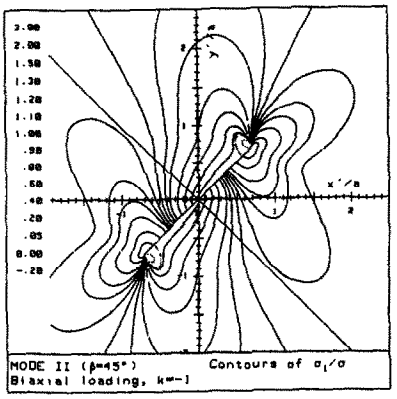
MODE II (β=45°) Contours of σ_1/σ
Biaxial loading, k=-1

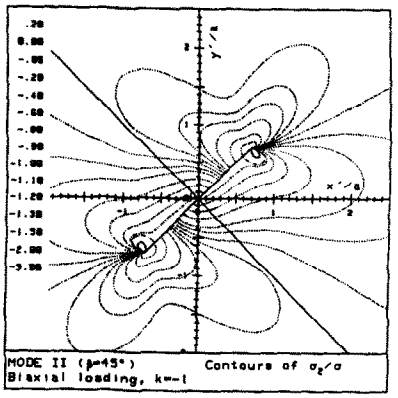
MODE II (β=45°) Contours of σ_θ/σ
Biaxial loading, k=-1

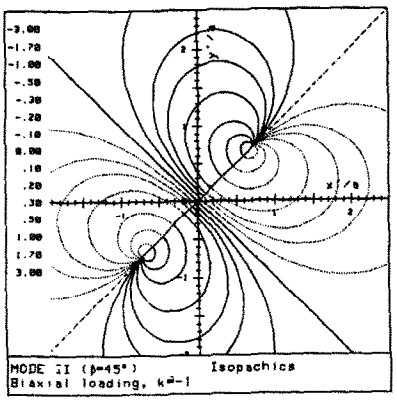
MODE II (β=45°) Isopachics
Biaxial loading, k=-1

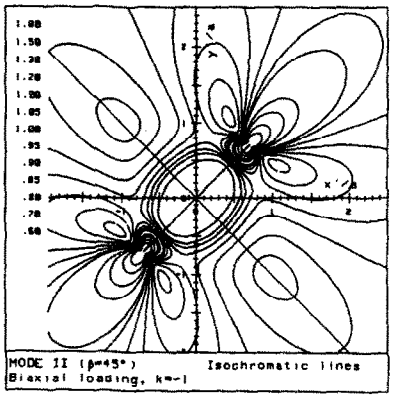
MODE II (β=45°) Isochromatic lines
Biaxial loading, k=-1

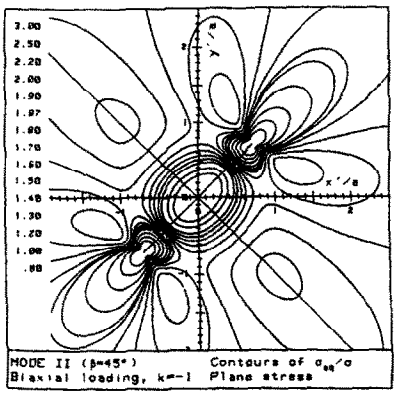
MODE II (β=45°) Contours of σ_{eq}/σ
Biaxial loading, k=-1 Plane stress

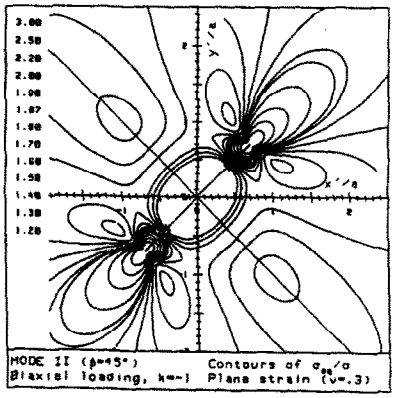
MODE II (β=45°) Contours of σ_{eq}/σ
Biaxial loading, k=-1 Plane strain (ν=.3)

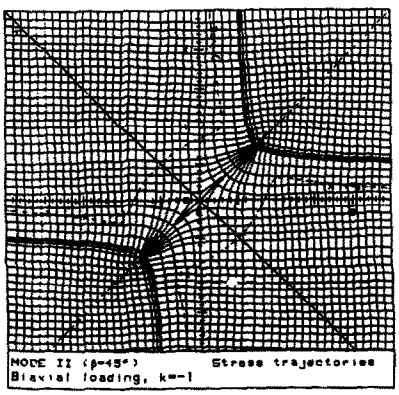
MODE II (β=45°) Stress trajectories
Biaxial loading, k=-1

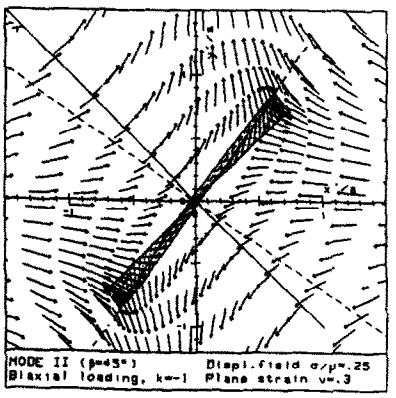
MODE II (β=45°) Displ.field σ/μ=.25
Biaxial loading, k=-1 Plane strain ν=.3

Fig. 15

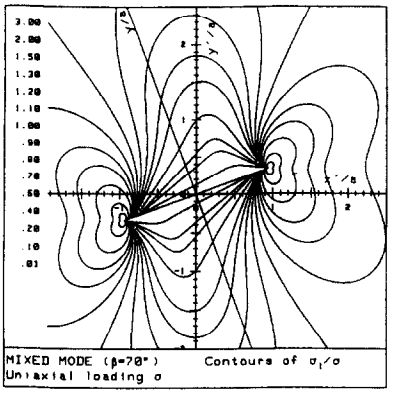
MIXED MODE (β=70°)
Uniaxial loading σ
Contours of σ1/σ

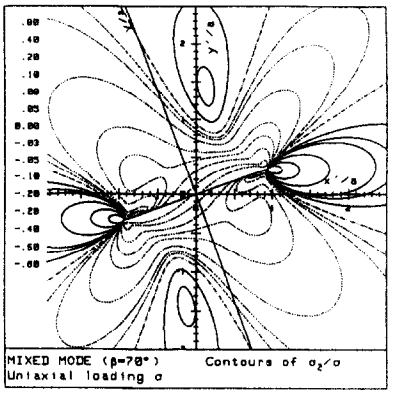
MIXED MODE (β=70°)
Uniaxial loading σ
Contours of σ2/σ

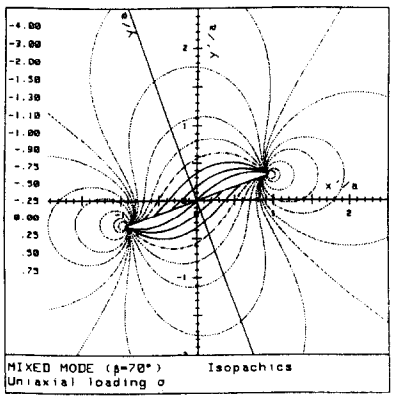
MIXED MODE (β=70°)
Uniaxial loading σ
Isopachics

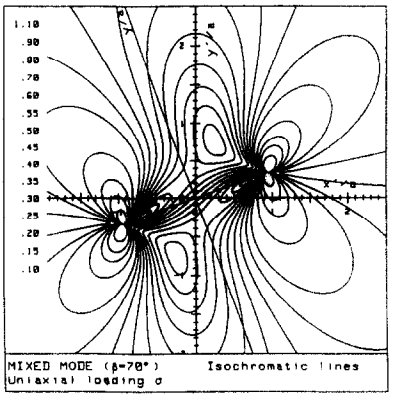
MIXED MODE (β=70°)
Uniaxial loading σ
Isochromatic lines

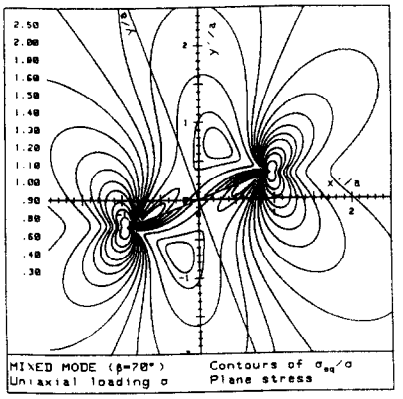
MIXED MODE (β=70°)
Uniaxial loading σ
Contours of σeq/σ
Plane stress

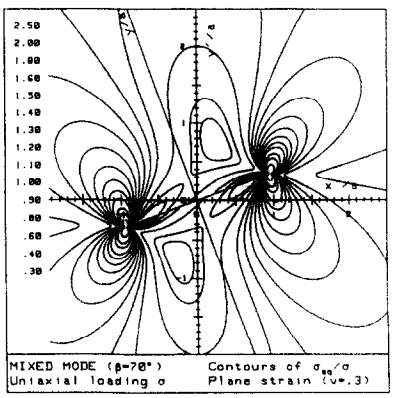
MIXED MODE (β=70°)
Uniaxial loading σ
Contours of σeq/σ
Plane strain (ν=.3)

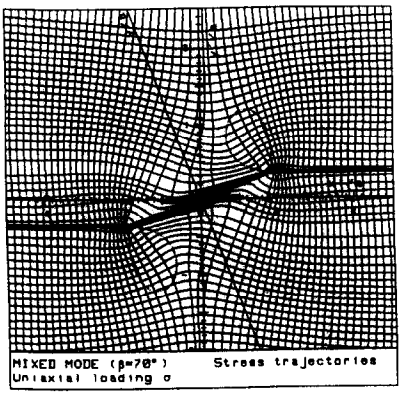
MIXED MODE (β=70°)
Uniaxial loading σ
Stress trajectories

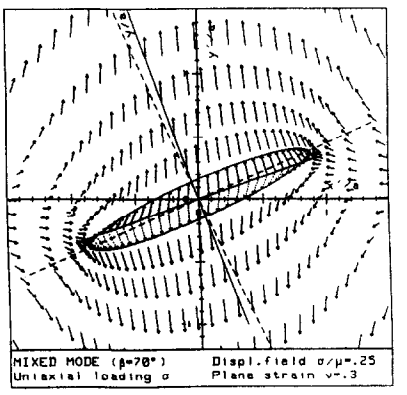
MIXED MODE (β=70°)
Uniaxial loading σ
Displ.field σ/μ=.25
Plane strain ν=.3

Fig. 16

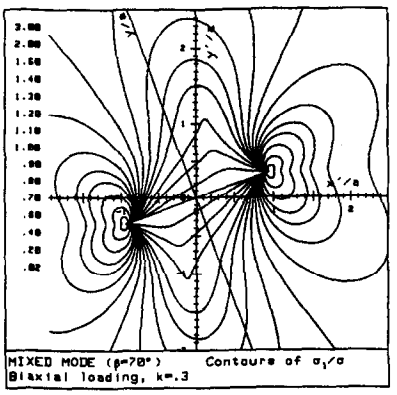
MIXED MODE (β=70°) Contours of σ1/σ
Biaxial loading, k=.3

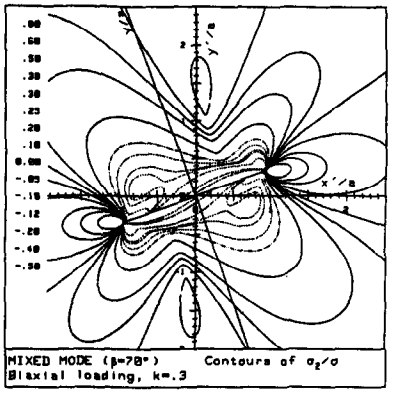
MIXED MODE (β=70°) Contours of σ2/σ
Biaxial loading, k=.3

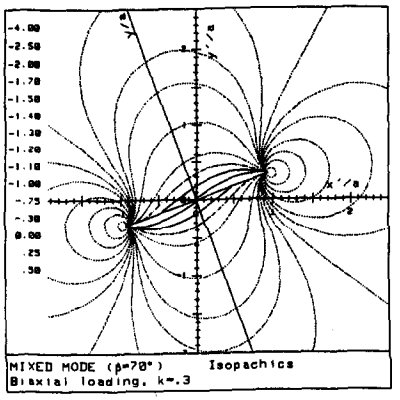
MIXED MODE (β=70°) Isopachics
Biaxial loading, k=.3

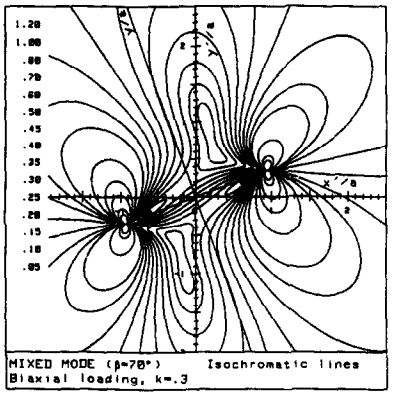
MIXED MODE (β=70°) Isochromatic lines
Biaxial loading, k=.3

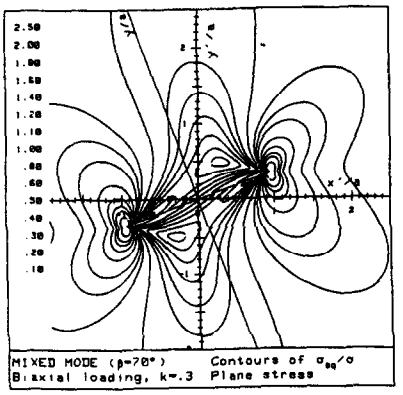
MIXED MODE (β=70°) Contours of σeq/σ
Biaxial loading, k=.3 Plane stress

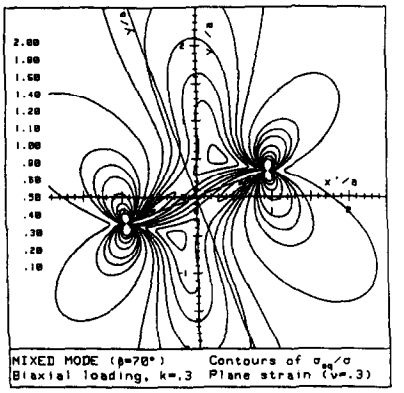
MIXED MODE (β=70°) Contours of σeq/σ
Biaxial loading, k=.3 Plane strain (ν=.3)

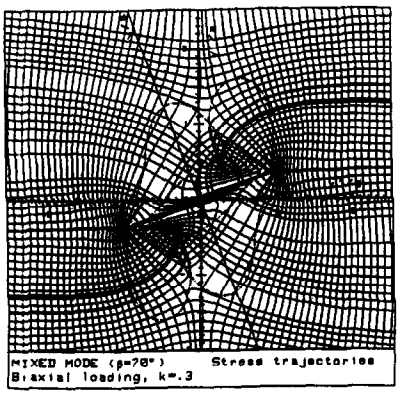
MIXED MODE (β=70°) Stress trajectories
Biaxial loading, k=.3

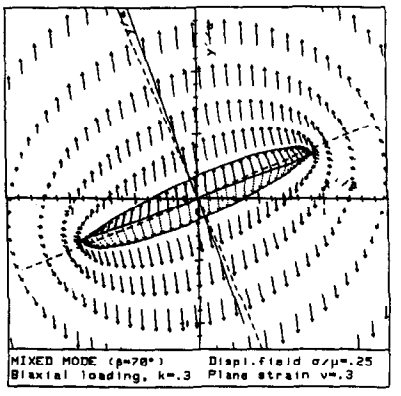
MIXED MODE (β=70°) Displ.field σ/μ=.25
Biaxial loading, k=.3 Plane strain ν=.3

Fig. 17

with + sign for the upper lip and − sign for the lower lip. Equations (125) and (126) have been found directly by Theocaris *et al.* [35].

On the y-axis (perpendicular to the crack) where $Q = T = V = 0$

$$(\sigma_y)_{x=0} = \frac{\sigma}{2}(m - n\cos 2\beta)\left(\frac{y^2}{y^2 + a^2}\right)^{3/2} \tag{127}$$

$$(\sigma_x)_{x=0} = \frac{\sigma}{2}(m - n\cos 2\beta)\frac{|y|}{(y^2 + a^2)^{3/2}}(y^2 + 2a^2) + \sigma n\cos 2\beta \tag{128}$$

$$(\tau_{xy})_{x=0} = \frac{\sigma}{2} n\sin 2\beta \frac{|y|}{(y^2 + a^2)^{3/2}}(y^2 + 2a^2) \tag{129}$$

$$(u_x)_{x=0} = \text{sign(y)}\frac{\sigma}{8\mu} n\sin 2\beta\left[-(\kappa + 1)|y| + \left(\kappa + 1 + \frac{2y^2}{y^2 + a^2}\right)\sqrt{(y^2 + a^2)}\right] \tag{130}$$

$$(u_y)_{x=0} = \text{sign(y)}\frac{\sigma}{8\mu}\left[n\cos 2\beta(\kappa - 3)|y| + (m - n\cos 2\beta)\left(\kappa + 1 - \frac{2y^2}{y^2 + a^2}\right)\sqrt{(y^2 + a^2)}\right]. \tag{131}$$

5.1. *Displacements*

The discontinuities of displacements of a point x, y of the crack lips (between $y = 0+$ and $y = 0-$) is, from eqs (125) and (126),

$$[u_x] = \frac{\kappa + 1}{4\mu}\sigma n\sin 2\beta(a^2 - x^2)^{1/2} \tag{132}$$

$$[u_y] = \frac{\kappa + 1}{4\mu}\sigma(m - n\cos 2\beta)(a^2 - x^2)^{1/2}. \tag{133}$$

From eqs (89), (90) and (84), the deformed crack is an ellipse of semi-axes

$$a' = \frac{a}{2}|1 + mS + \sqrt{H}| \tag{134}$$

$$b' = \frac{a}{2}|1 + mS - \sqrt{H}| \tag{135}$$

turned by an angle α defined by

$$\sin 2\alpha = \frac{2Sn\sin 2\beta}{\sqrt{H}} \tag{136}$$

where

$$H = (1 - mS)^2 + 4nS(1 - mS)\cos 2\beta + 4n^2S^2 \tag{137a}$$

$$= [1 + mS - 2S(m - n\cos 2\beta)]^2 + [2Sn\sin 2\beta]^2. \tag{137b}$$

The lips interfere if

$$S[(m - n\cos 2\beta) - nS(n - m\cos 2\beta)] < 0. \tag{138}$$

They are just in contact if $S = 0$ (initial position) or

$$\cos 2\beta = \frac{n^2S - m}{n(m - 1)}. \tag{139}$$

Equations (134), (135), (136) and (139) have been derived directly by Theocaris *et al.* [35]. As pointed out by Theocaris [33], the points on the ellipse where the initial crack tips move after deformation do not coincide in general with the points of maximum curvature of the ellipse.

In the particular case of mode II ($\beta = 45°$, $k = -1$) one has

$$a' = \frac{a}{2}(1 + \sqrt{(1 + 16S^2)})$$

$$b' = \frac{a}{2}(1 - \sqrt{(1 + 16S^2)})$$

and interpenetration would occur as soon as $\sigma \neq 0$, as shown in Fig. 15 where displacements of the lower lip are shown as a dotted line.

These problems of overlapping have been discussed in detail by Theocaris [31, 32, 34, 36]. However, as discussed above, second order terms must be dropped out in linearized elasticity, so that the results are

$$a' = a(1 + Sn \cos 2\beta) \tag{140}$$

$$b' = aS(m - n \cos 2\beta) \tag{141}$$

$$\sin 2\alpha = 2Sn \sin 2\beta \tag{142}$$

and the condition of non-interpenetration is simply $K_I \geqslant 0$.

5.2. *Approximations*

Let us study stresses and displacement in the neighbourhood of the crack tip, by letting

$$x = a + r \cos\theta$$

$$y = r \sin\theta,$$

where $0 < r/a \ll 1$. We have

$$\sqrt{\Delta} \sim 2\frac{r}{a} + \frac{r^2}{a^2}\cos\theta \tag{143}$$

$$U \sim \left(\frac{2r}{a}\right)^{1/2} \sin\frac{\theta}{2}\left[1 + \frac{r}{4a}(2\cos\theta + 1)\right] \tag{144}$$

$$V \sim \left(\frac{2r}{a}\right)^{1/2} \cos\frac{\theta}{2}\left[1 + \frac{r}{4a}(2\cos\theta - 1)\right] \tag{145}$$

$$2\lambda(\cosh 2\xi - 1) \sim 2\cos^2\frac{\theta}{2} + \frac{r}{2a}\sin^2\theta \tag{146}$$

$$R \sim 2\left(\frac{a}{2r}\right)^{1/2} \cos\frac{\theta}{2} + \frac{3}{2}\left(\frac{r}{2a}\right)^{1/2} \cos\frac{\theta}{2} \tag{147}$$

$$T \sim 2\left(\frac{a}{2r}\right)^{1/2} \sin\frac{\theta}{2} - \frac{3}{2}\left(\frac{r}{2a}\right)^{1/2} \sin\frac{\theta}{2} \tag{148}$$

$$P \sim \left(\frac{a}{2r}\right)^{1/2} \sin\frac{\theta}{2}\cos\frac{\theta}{2}\sin\frac{3\theta}{2} - \frac{3}{4}\left(\frac{r}{2a}\right)^{1/2} \cos\frac{\theta}{2}\sin^2\frac{\theta}{2} \tag{149}$$

$$Q \sim \left(\frac{a}{2r}\right)^{1/2} \sin\frac{\theta}{2}\cos\frac{\theta}{2}\cos\frac{3\theta}{2} - \frac{3}{4}\left(\frac{r}{2a}\right)\sin\frac{\theta}{2}\cos^2\frac{\theta}{2}. \tag{150}$$

Introducing K_I and K_{II}, eqs (1) and (2), we easily obtain

$$\sigma_x = \sigma n \cos 2\beta + \frac{1}{\sqrt{(2\pi r)}}\left[K_I \cos\frac{\theta}{2}\left(1 - \sin\frac{\theta}{2}\sin\frac{3\theta}{2}\right) - K_{II}\sin\frac{\theta}{2}\left(2 + \cos\frac{\theta}{2}\cos\frac{3\theta}{2}\right)\right]$$
$$+ \frac{3}{8a}\sqrt{\left(\frac{r}{2\pi}\right)}\left[K_I \cos\frac{\theta}{2}(3 - \cos\theta) + K_{II}\sin\frac{\theta}{2}(5 + \cos\theta)\right] \tag{151}$$

$$\sigma_y = \frac{\cos\frac{\theta}{2}}{\sqrt{(2\pi r)}}\left[K_I\left(1 + \sin\frac{\theta}{2}\sin\frac{3\theta}{2}\right) + K_{II}\sin\frac{\theta}{2}\cos\frac{3\theta}{2}\right]$$
$$+ \frac{3}{8a}\sqrt{\left(\frac{r}{2\pi}\right)}\cos\frac{\theta}{2}[K_I(1 + \cos\theta) - K_{II}\sin\theta] \tag{152}$$

$$\tau_{xy}=\frac{\cos\frac{\theta}{2}}{\sqrt{(2\pi r)}}\left[K_{\mathrm{I}}\sin\frac{\theta}{2}\cos\frac{3\theta}{2}+K_{\mathrm{II}}\left(1-\sin\frac{\theta}{2}\sin\frac{3\theta}{2}\right)\right]$$

$$-\frac{3}{8a}\sqrt{\left(\frac{r}{2\pi}\right)}\cos\frac{\theta}{2}[K_{\mathrm{I}}\sin\theta-K_{\mathrm{II}}(3-\cos\theta)] \quad (153)$$

$$2\mu u_x=\frac{\sigma}{4}(\kappa+1)(xn\cos 2\beta-yn\sin 2\beta)$$

$$+\sqrt{\left(\frac{r}{2\pi}\right)}\left[K_{\mathrm{I}}(\kappa-\cos\theta)\cos\frac{\theta}{2}+K_{\mathrm{II}}(\kappa+\cos\theta+2)\sin\frac{\theta}{2}\right]$$

$$+\frac{\pi}{2a}\left(\frac{r}{2\pi}\right)^{3/2}\left\{K_{\mathrm{I}}\left[(\kappa+1)\cos\frac{3\theta}{2}-2\cos^3\frac{\theta}{2}\right]+K_{\mathrm{II}}\left[(\kappa+1)\sin\frac{3\theta}{2}+3\sin\theta\cos\frac{\theta}{2}\right]\right\} \quad (154)$$

$$2\mu u_y=\frac{\sigma}{4}[(\kappa-3)yn\cos 2\beta+(\kappa+1)xn\sin 2\beta]$$

$$+\sqrt{\left(\frac{r}{2\pi}\right)}\left[K_{\mathrm{I}}(\kappa-\cos\theta)\sin\frac{\theta}{2}-K_{\mathrm{II}}(\kappa+\cos\theta-2)\cos\frac{\theta}{2}\right]$$

$$+\frac{\pi}{2a}\left(\frac{r}{2\pi}\right)^{3/2}\left\{K_{\mathrm{I}}\left[(\kappa-1)\sin\frac{3\theta}{2}-2\sin^3\frac{\theta}{2}\right]-K_{\mathrm{II}}\left[(\kappa-1)\cos\frac{3\theta}{2}+3\sin\theta\sin\frac{\theta}{2}\right]\right\}. \quad (155)$$

The two-term approximation for stresses and the one-term expression for displacement were obtained directly by Eftis and Subramonian [24] with an error in u_x later corrected by Smith [51]. Finally, the above eqs (151)–(153) were obtained by Theocaris and Spyropoulos [25] who used them to derive an expression for the maximum shear stress τ_m.

Expressed in polar coordinates, these stresses are as follows:

$$\sigma_r=\sigma n\cos 2\beta\cos^2\theta+\frac{1}{2\sqrt{(2\pi r)}}\left[K_{\mathrm{I}}\cos\frac{\theta}{2}(3-\cos\theta)+K_{\mathrm{II}}\sin\frac{\theta}{2}(3\cos\theta-1)\right]$$

$$+\frac{3}{8a}\sqrt{\left(\frac{r}{2\pi}\right)}\left[K_{\mathrm{I}}\cos\frac{\theta}{2}(1-\cos\theta+2\cos^2\theta)+K_{\mathrm{II}}\sin\frac{\theta}{2}(10\cos^2\theta+5\cos\theta-1)\right] \quad (156)$$

$$\sigma_\theta=\sigma n\cos 2\beta\sin^2\theta+\frac{\cos\frac{\theta}{2}}{2\sqrt{(2\pi r)}}[K_{\mathrm{I}}(1+\cos\theta)-3K_{\mathrm{II}}\sin\theta]$$

$$+\frac{3}{8a}\sqrt{\left(\frac{r}{2\pi}\right)}\cos\frac{\theta}{2}[K_{\mathrm{I}}(1+\cos\theta)(3-2\cos\theta)+5K_{\mathrm{II}}(1-2\cos\theta)\sin\theta] \quad (157)$$

$$\tau_{r\theta}=-\sigma n\cos 2\beta\sin\theta\cos\theta+\frac{\cos\frac{\theta}{2}}{2\sqrt{(2\pi r)}}[K_{\mathrm{I}}\sin\theta+K_{\mathrm{II}}(3\cos\theta-1)]$$

$$+\frac{3}{8a}\sqrt{\left(\frac{r}{2\pi}\right)}\cos\frac{\theta}{2}[K_{\mathrm{I}}\sin\theta(1-2\cos\theta)+K_{\mathrm{II}}(10\cos^2\theta-5\cos\theta-3)]. \quad (158)$$

Approximations with one, two and three terms are depicted in Figs 18–20 for uniaxial mode I, and are to be compared to the exact solution, Fig. 13.

5.3. *Angled crack*

The slope of the stress trajectories at a point x,y is given by

$$\tan 2\gamma=-\frac{2\tau_{xy}}{\sigma_y-\sigma_x}. \quad (159)$$

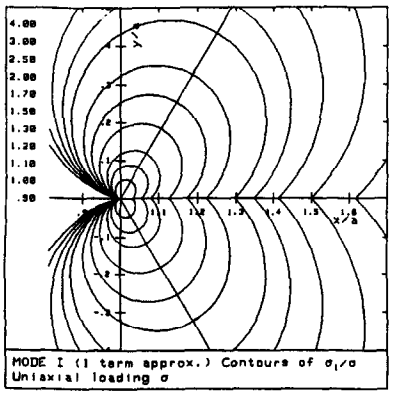
MODE I (1 term approx.) Contours of σ_1/σ
Uniaxial loading σ

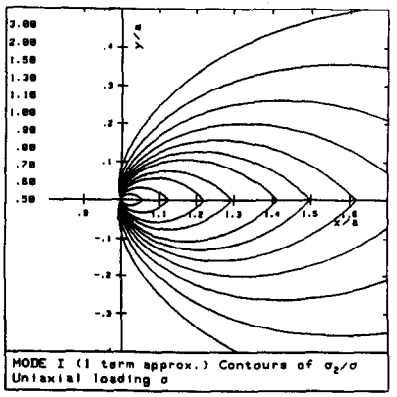
MODE I (1 term approx.) Contours of σ_2/σ
Uniaxial loading σ

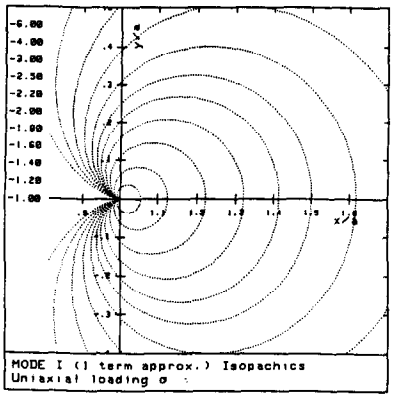
MODE I (1 term approx.) Isopachics
Uniaxial loading σ

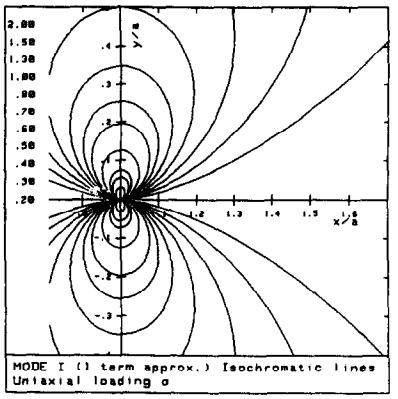
MODE I (1 term approx.) Isochromatic lines
Uniaxial loading σ

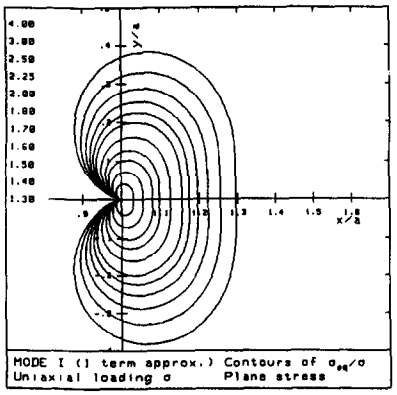
MODE I (1 term approx.) Contours of σ_{ee}/σ
Uniaxial loading σ Plane stress

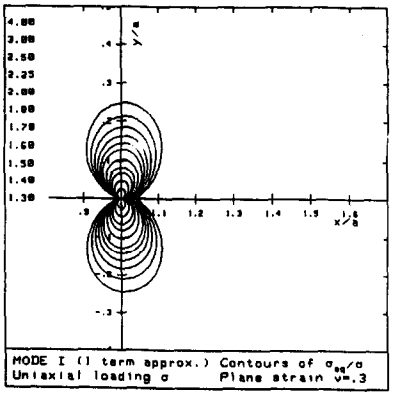
MODE I (1 term approx.) Contours of σ_{ee}/σ
Uniaxial loading σ Plane strain ν=.3

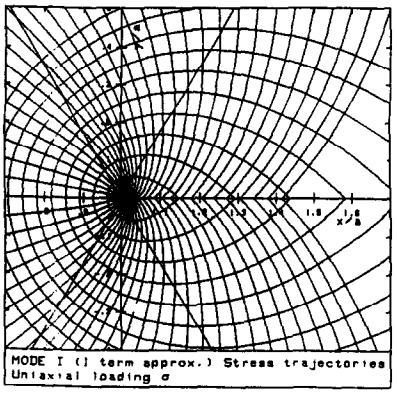
MODE I (1 term approx.) Stress trajectories
Uniaxial loading σ

Fig. 18

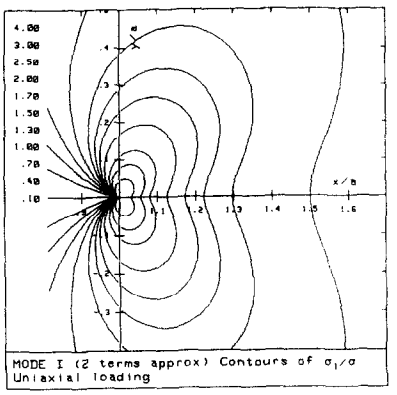
MODE I (2 terms approx) Contours of σ_1/σ
Uniaxial loading

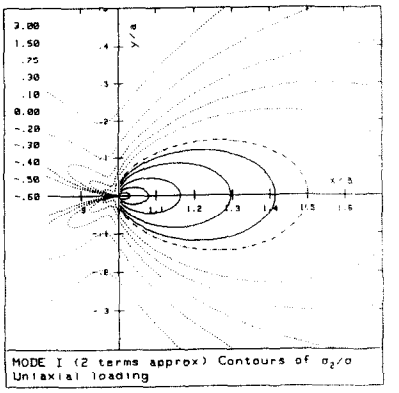
MODE I (2 terms approx) Contours of σ_2/σ
Uniaxial loading

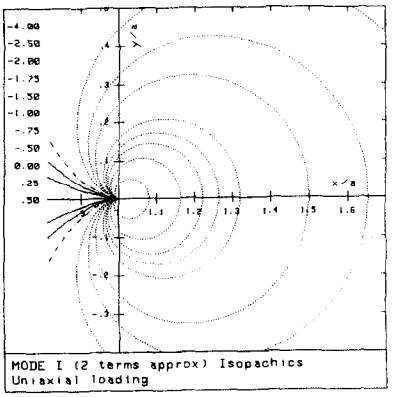
MODE I (2 terms approx) Isopachics
Uniaxial loading

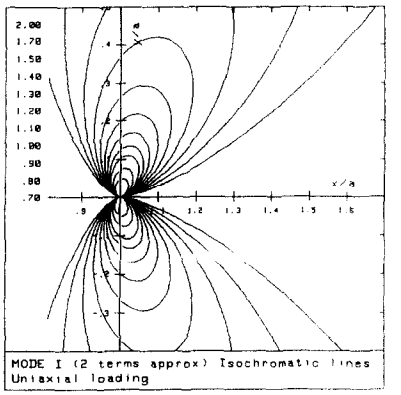
MODE I (2 terms approx) Isochromatic lines
Uniaxial loading

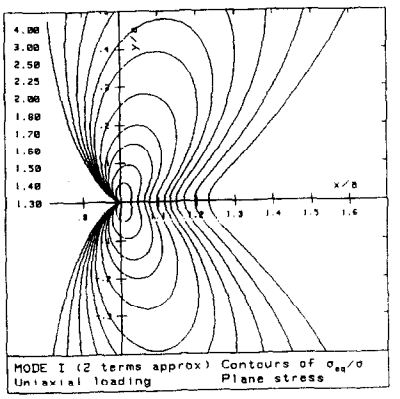
MODE I (2 terms approx) Contours of σ_{eq}/σ
Uniaxial loading Plane stress

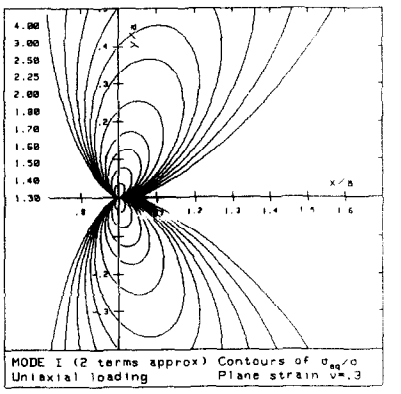
MODE I (2 terms approx) Contours of σ_{eq}/σ
Uniaxial loading Plane strain ν=.3

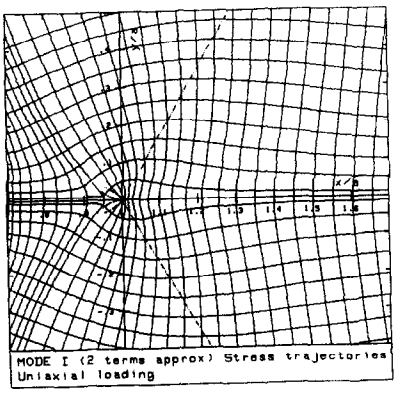
MODE I (2 terms approx) Stress trajectories
Uniaxial loading

Fig. 19

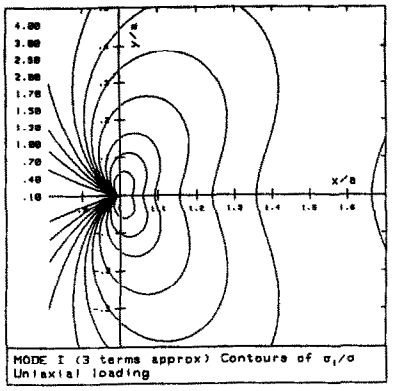
MODE I (3 terms approx) Contours of σ_1/σ
Uniaxial loading

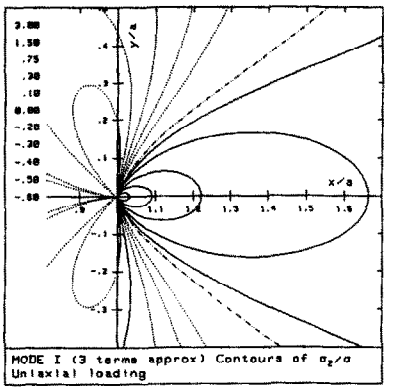
MODE I (3 terms approx) Contours of σ_2/σ
Uniaxial loading

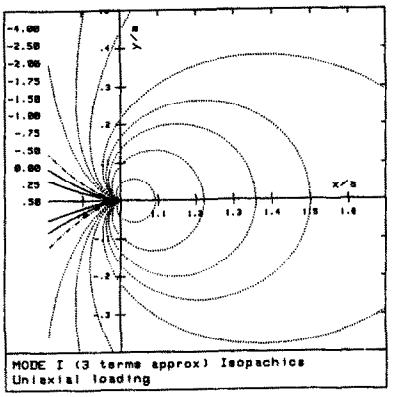
MODE I (3 terms approx) Isopachics
Uniaxial loading

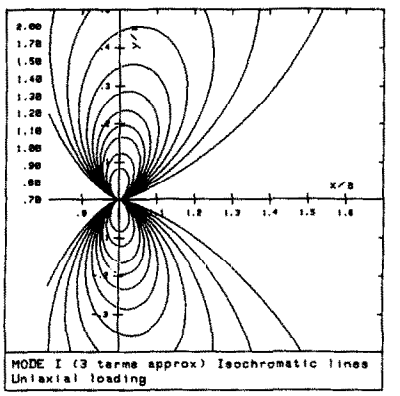
MODE I (3 terms approx) Isochromatic lines
Uniaxial loading

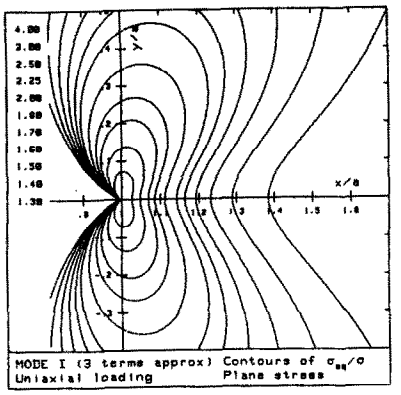
MODE I (3 terms approx) Contours of σ_{zz}/σ
Uniaxial loading Plane stress

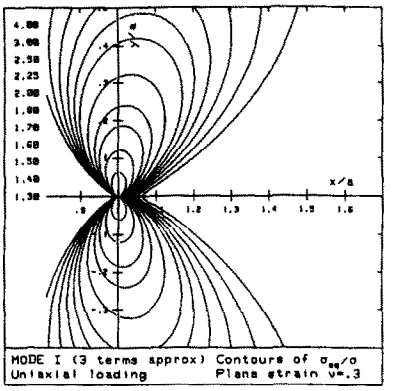
MODE I (3 terms approx) Contours of σ_{zz}/σ
Uniaxial loading Plane strain ν=.3

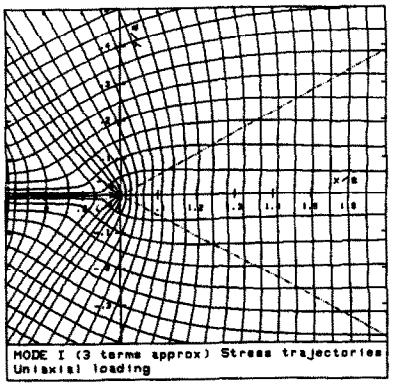
MODE I (3 terms approx) Stress trajectories
Uniaxial loading

Fig. 20

For $r = 0$, the angle γ is the angle θ of polar coordinates, and from eqs (151)–(153) we have rigorously

$$\tan\frac{\theta}{2}\frac{K_I\sin\theta(2\cos\theta+1)+K_{II}(2\cos^2\theta+1+\cos\theta)}{K_I\sin\theta(2\cos\theta-1)+K_{II}(2\cos^2\theta+1-\cos\theta)}+\frac{1-\tan^2\theta}{2\tan\theta}=0, \tag{160}$$

i.e.

$$[K_I\sin\theta+K_{II}(3\cos\theta-1)](1+\tan^2\theta)=0. \tag{161}$$

The initial slope of the stress trajectory starting from the crack tip is thus given by

$$K_I\sin\theta+K_{II}(3\cos\theta-1)=0, \tag{162}$$

i.e.

$$\tan\frac{\theta}{2}=\frac{K_I-\sqrt{(K_I^2+8K_{II}^2)}}{4K_{II}} \tag{163}$$

or for $|K_{II}/K_I| \ll 1$ ($\beta \to 90°$ or $\beta \to 0$ in biaxial loading)

$$\theta \sim -\frac{2K_{II}}{K_I}. \tag{164}$$

For $k > 0$, the initial slope has a maximum at

$$\cos 2\beta = \frac{n}{m} \tag{165}$$

whose value is

$$\tan\frac{\theta_m}{2}=\frac{\sqrt{k}-\sqrt{(2k^2-3k+2)}}{2|1-k|}. \tag{166}$$

For uniaxial loading, eq. (162) becomes

$$\tan\beta-\frac{1-3\cos\theta}{\sin\theta}=0 \tag{167}$$

and the maximum $\theta_m = -70°53'$ is found for $\beta = 0$.

Note that making $\xi_0 = 0$ in eq. (75) giving the initial slope for an ellipse would lead to

$$\tan\gamma=\frac{K_I-\sqrt{(K_I^2+K_{II}^2)}}{K_{II}},$$

i.e. for uniaxial loading

$$-\gamma=\frac{\pi}{4}-\frac{\beta}{2}$$

as given by McClintock [52], and

$$\gamma=-\frac{K_{II}}{2K_I}$$

for small K_{II}/K_I. This result is not correct, since $\cosh 2\xi_0 - \cos 2\eta$ was assumed to be non-zero in the derivative of σ_η, eq. (71). There is thus a discontinuity in the initial slope for $\xi_0 = 0$.

Equation (162) is the Erdogan and Sih [53] criterion. Using the one-term approximation for σ_θ and $\tau_{r\theta}$, eqs (157) and (158), they proposed that the angled crack will run in a direction given by $\partial\sigma_\theta/\partial\theta = 0$ (maximum tangential stress criterion, MTS). As $\tau_{r\theta} = 0$ in this direction, it is the initial slope of the stress trajectory.

Later Williams and Ewing [54] used the two-term approximation for σ_θ and wrote the MTS criterion at a distance r/a. They found, for uniaxial loading, and after a correction by Finnie and Saith [55], the criterion

$$\tan^2\beta-\frac{1-3\cos\theta}{\sin\theta}\tan\beta-\sqrt{\left(\frac{2r}{a}\right)}\frac{16\sin\frac{\theta}{2}}{3\tan\theta}(1-\tan^2\beta)=0, \tag{168}$$

(a)

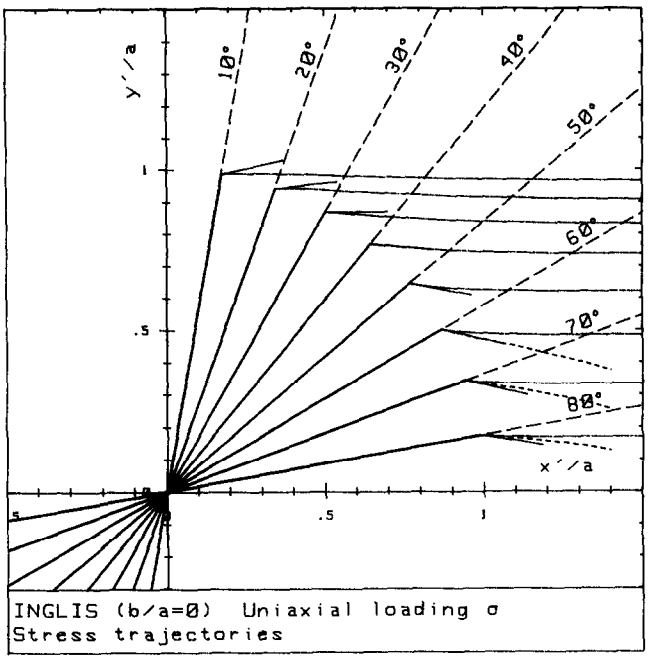

(b)

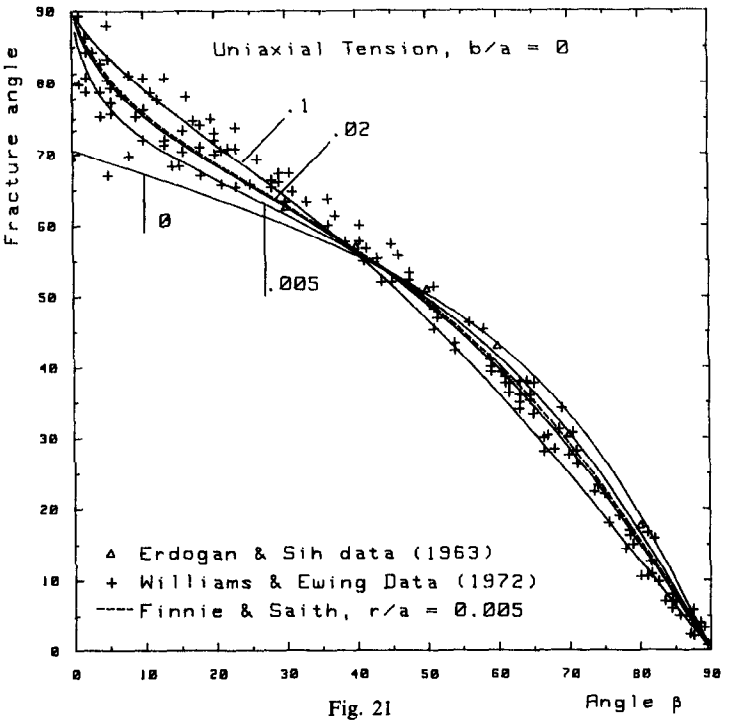

Fig. 21

which gave a good fit to experimental data for $r/a = 0.005$. However, $\tau_{r\theta}$ is not zero in this direction, for the condition $\tau_{r\theta} = 0$ is

$$\tan^2\beta - \frac{1-3\cos\theta}{\sin\theta}\tan\beta - \sqrt{\left(\frac{2r}{a}\right)}\frac{4\sin\frac{\theta}{2}}{\tan\theta}(1-\tan^2\beta) = 0. \tag{169}$$

As the stress trajectory starting from the crack tip turns rapidly, its tangent at a distance r/a is not directed towards the crack tip, and eq. (169) corresponds to a stress trajectory which does not reach the crack tip. In fact, for an angle θ, the right stress trajectory passes at a distance larger than that indicated by eqs (168) and (169).

Note that Cotterell and Rice [27] found the Erdogan and Sih [53] criterion by another method. They computed the stress intensity factors k_1 and k_2 at the tip of an infinitesimally small kink making an angle θ with the main crack, and found (after evident simplification)

$$k_1 = \tfrac{1}{2}\cos\frac{\theta}{2}[K_I(1+\cos\theta) - 3K_{II}\sin\theta] \tag{170}$$

$$k_2 = \tfrac{1}{2}\cos\frac{\theta}{2}[K_I\sin\theta + K_{II}(3\cos\theta - 1)]. \tag{171}$$

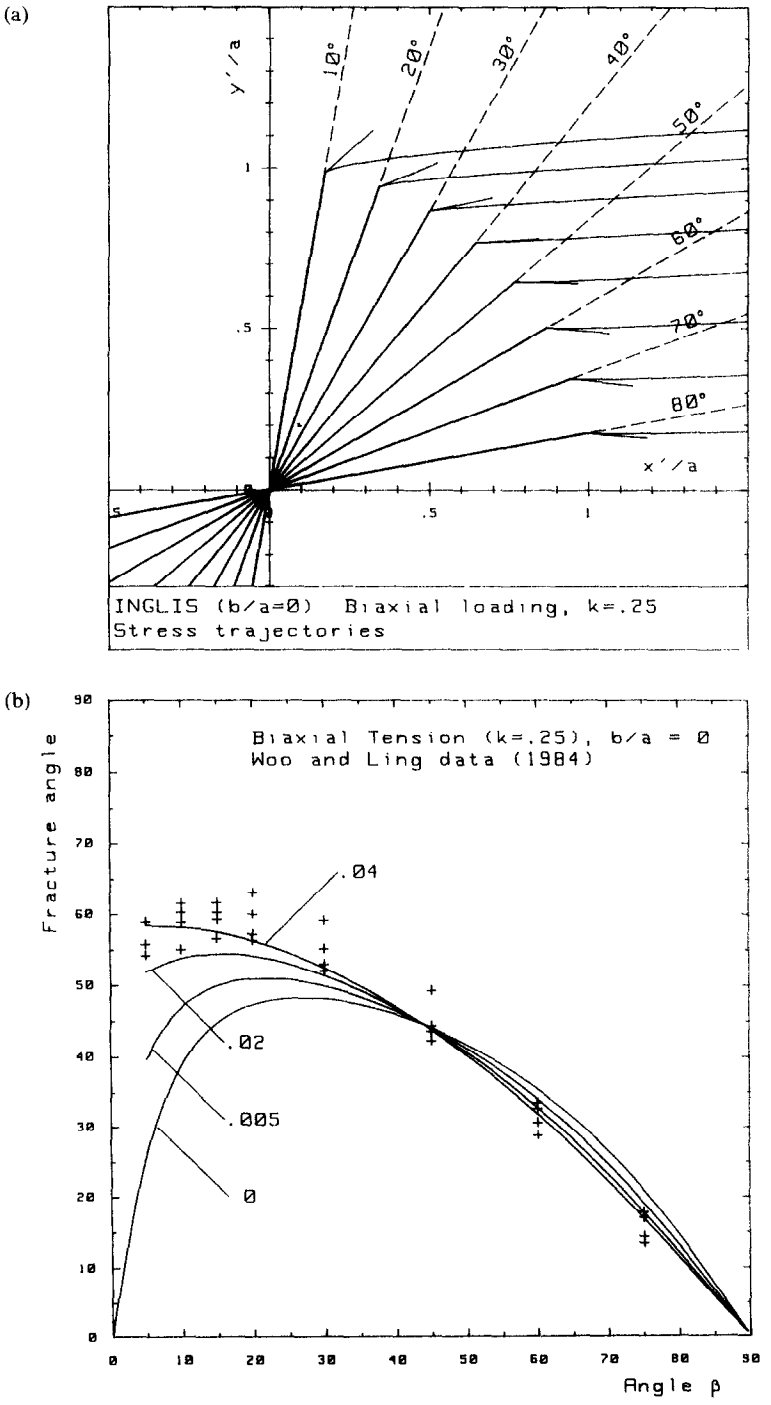

Fig. 22

These expressions are identical to the singular terms of σ_θ, and $\tau_{r\theta}$, eqs (157) and (158), and their condition of local symmetry ($k_2 = 0$) gives eq. (162) together with $\partial k_1/\partial\theta = 0$.

In Figs 21a and 22a we have drawn the stress trajectories starting from the crack tip for uniaxial tension ($k = 0$) and biaxial tension ($k = 0.25$). The initial slope is shown by a small segment, and the first point of the stress trajectory is taken on it at a distance $r/a = 10^{-5}$ to avoid division by zero.

The mean slopes of the stress trajectories computed between the crack tip and a point of the trajectory taken at various distances r/a, are compared to the experimental results of Erdogan and Sih [53] and Williams and Ewing [54] for an angled crack in uniaxial tension (Fig. 21b) and to those of Woo and Ling [56] for biaxial tension with $k = 0.25$ (Fig. 22b). Experimental results are in agreement with angles measured at a distance between $r/a = 0.005$ and $r/a = 0.1$. (Using a protractor for measuring the angles in Fig. 21a gives, approximately, the curve for $r/a = 0.1$.) In Fig. 21b, the Finnie and Saith equation, eq. (168), with their empirical value $r/a = 0.005$ (dashed line), is quite identical to the mean slope of the stress trajectories measured at $r/a = 0.02$.

Sumi *et al.* [29] gave the angled crack trajectory in the form

$$y = \alpha'(x-1) + \beta'(x-1)^{3/2} + \gamma'(x-1)^2, \tag{172}$$

where for large angles β (small K_{II})

$$\alpha' = -\frac{2K_{II}}{K_I}$$

$$\beta' = \frac{8\alpha'}{3}\sqrt{\left(\frac{2}{\pi}\right)}\frac{\sigma n \cos 2\beta}{K_I}$$

$$\gamma' = \alpha'\left(\frac{1}{4a} + \frac{4\sigma^2 n^2 \cos^2 2\beta}{K_I^2}\right).$$

For uniaxial loading, this crack trajectory

$$Y = -\frac{2}{\tan\beta}\left\{X - 1 + \frac{2\sqrt{2}}{3\pi}\left(\frac{4\cos 2\beta}{\sin^2\beta}\right)(X-1)^{3/2} + \frac{1}{4}\left[1 + \frac{1}{\pi}\left(\frac{4\cos 2\beta}{\sin^2\beta}\right)^2\right](X-1)^2\right\} \tag{173}$$

is shown as a dotted line in Fig. 21a, for $\beta \geqslant 60°$.

6. CONCLUSION

The stress tensor given by Chang and Wu [13] was depicted by drawing contours of principal stresses, isopachics, isochromatic lines, the von Mises criterion and stress trajectories for both elliptical cavities and cracks. For a crack this stress tensor is written in Cartesian coordinates, and simple expressions are given for mode I.

Published experimental results on angled cracks in uniaxial tension or compression are in agreement with the slope of the stress trajectory starting from the crack tip or the more stressed point of the cavity.

An error in the Stevenson [8] complex potentials, leading to wrong results for displacements, is corrected and the displacement field around cavities or cracks is depicted. The shape of the deformed crack is in agreement with the one computed directly by Theocaris *et al.* [35]. However, in the framework of linearized elasticity, no conclusion can be drawn on the overlapping of crack lips found by the exact calculation when it is due to second order effects.

The use of the exact solutions is by no means more difficult than the use of two- or three-term approximations for drawing the various contours and the stress trajectories.

Acknowledgements—Thanks are due to V. I. Fabrikant for fruitful discussions and to C. Stefani who has checked all the calculations.

REFERENCES

[1] C. E. Inglis, Stresses in a plate due to the presence of cracks and sharp corners. *Trans. Inst. nav. Arch.* **55**, 219–241 (1913).

[2] A. A. Griffith, The phenomena of rupture and flow in solids. *Phil. Trans. R. Soc.* **A221,** 163–198 (1920).
[3] T. Pöschl, Uber eine particular lösung des biharmonischen problems für den AnBeuraum einer Ellipse. *Math. Z.* **11,** 89–96 (1921).
[4] K. Wolf, Beitrage zur ebener Elastizitätstheorie. *Z. tech. Phys.* **2,** 209–216 (1921).
[5] N. I. Muskhelishvili, Sur la solution du problème biharmonique pour l'aire extérieure à une ellipse. *Math Z.* **26,** 700–705 (1927).
[6] N. I. Muskhelishvili, *Some Basic Problems of the Mathematical Theory of Elasticity*. Noordhoff, Leyden (1975).
[7] L. Föpl, Konforme Abbildung ebener Spannungszustände. *Z. angnew. Math. Mech.* **11,** 81–92 (1931).
[8] A. C. Stevenson, Complex potentials in two-dimensional analysis. *Proc. R. Soc.* **A184,** 129–179 (1945).
[9] S. Timoshenko and J. N. Goodier, *Theory of Elasticity*. McGraw-Hill, New York (1951).
[10] H. Neuber, *Kerbspannungslehre*. Springer, Berlin (1958).
[11] J. C. Jaeger and N. G. W. Cook, *Fundamentals of Rock Mechanics*. Methuen, London (1969).
[12] H. C. Wu and K. J. Chang, Angled elliptic notch problem in compression and tension. *J. appl. Mech.* **45,** 258–262 (1978).
[13] K. J. Chang and H. C. Wu, Angled elliptic notch problem under biaxial loading. *J. appl. Mech.* **47,** 57–63 (1980).
[14] H. Küppers, Die numerische Berechnung der Spannungsverteilung in die Umgebung einer Kerbspilze. *Glasstech. Ber.* **37,** 185–189 (1964).
[15] I. N. Sneddon, The distribution of stresses in the neighbourhood of a crack in an elastic solid. *Proc. R. Soc.* **A187,** 229–260 (1946).
[16] H. W. Westergaard, Bearing pressure and cracks. *Trans. ASME* **61,** A49–A53 (1936).
[17] M. L. Williams, On the stress distribution on the base of a stationary crack. *J. appl. Mech.* **24,** 109–114 (1957).
[18] A. A. Wells and D. Post, The dynamic stress distribution surrounding a running crack. A photoelastic analysis. *Proc. SESA* **16,** 69–92 (1958).
[19] G. R. Irwin, Discussion of "The dynamic stress distribution surrounding a running crack. A photoelastic analysis". *Proc. SESA* **16,** 92–96 (1958).
[20] G. R. Irwin, Analysis of stresses and strains near the end of a crack traversing a plate. *J. appl. Mech.* **24,** 361–364 (1957).
[21] G. C. Sih, On the Westergaard method of crack analysis. *Int. J. Fracture* **2,** 628–631 (1966).
[22] J. Eftis and H. Liebowitz, On the modified Westergaard equations for certain plane crack problems. *Int. J. Fracture* **8,** 383–392 (1972).
[23] J. Eftis, N. Subramonian and H. Liebowitz, Crack border stress and displacement equations revisited. *Engng Fracture Mech.* **9,** 189–210 (1977).
[24] J. Eftis and N. Subramonian, The inclined crack under biaxial loading. *Engng Fracture Mech.* **10,** 43–67 (1978).
[25] P. S. Theocaris and C. P. Spyropoulos, Photoelastic determination of complex stress intensity factors for slant cracks under biaxial loading with higher order term effects. *Acta Mech.* **48,** 57–70 (1983).
[26] B. Cotterell, Notes on the paths and stability of cracks. *Int. J. Fracture* **2,** 526–533 (1966).
[27] B. Cotterell and J. R. Rice, Slightly curved or kinked cracks. *Int. J. Fracture* **16,** 155–169 (1980).
[28] Y. Sumi, S. Nemat-Nasser and L. M. Keer, On crack branching and curving in a finite body. *Int. J. Fracture* **21,** 67–79 (1983).
[29] Y. Sumi, S. Nemat-Nasser and L. M. Keer, On crack path stability in a finite body. *Engng Fracture Mech.* **22,** 759–771 (1985).
[30] P. S. Theocaris, The exact form and properties of the deformed transverse internal elastic crack. *Engng Fracture Mech.* **23,** 851–862 (1986).
[31] P. S. Theocaris, Displacement constraints of the faces of internal cracks due to pure shear. *Engng Fracture Mech.* **24,** 383–397 (1986).
[32] P. S. Theocaris, Paradoxes in the deformation modes of crack flanks due to shear. *Engng Fracture Mech.* **26,** 251–266 (1987).
[33] P. S. Theocaris, The internal crack in an extended or compressed plate: its geometric characteristics. *Engng Fracture Mech.* **26,** 753–770 (1987).
[34] P. S. Theocaris, In-plane stresses and strains along the flanks of internal elastic crack. *Engng Fracture Mech.* **30,** 145–159 (1988).
[35] P. S. Theocaris, D. Pazis and B. D. Konstantellos, The exact shape of a deformed internal slant crack under biaxial loading. *Int. J. Fracture* **30,** 135–153 (1986).
[36] D. Pazis, P. S. Theocaris and B. Konstantellos, Elastic overlapping of the crack flanks under mixed-mode loading. *Int. J. Fracture* **37,** 303–319 (1988).
[37] P. S. Theocaris, D. Pazis and B. D. Konstantellos, Elastic displacements along the flanks of internal cracks in rubber. *Exp. Mech.* **29,** 32–39 (1989).
[38] P. S. Theocaris, The topography around an internal crack: difference between exact and two-term solutions. *Engng Fracture Mech.* **33,** 707–717 (1989).
[39] M. E. Kipp and G. C. Sih, The strain energy density failure criterion applied to notched elastic solids. *Int. J. Solids Structures* **11,** 153–173 (1975).
[40] B. Cotterell, On brittle fracture paths. *Int. J. Fracture* **1,** 96–103 (1965).
[41] B. Cotterell, The paradox between the theories for tensile and compressive fracture. *Int. J. Fracture Mech.* **5,** 251–252 (1969).
[42] H. C. Wu, R. F. Yao and M. C. Yip, Experimental investigation of the angled elliptic notch problem in tension. *J. appl. Mech.* **44,** 455–461 (1977).
[43] B. Cotterell, Brittle fracture in compression. *Int. J. Fracture Mech.* **8,** 195–208 (1972).
[44] R. Mouginot and D. Maugis, Fracture indentation beneath flat and spherical punches. *J. Mater. Sci.* **20,** 4354–4376 (1985).
[45] K. J. Chang, Further studies of the maximum stress criterion of the angled crack problem. *Engng Fracture Mech.* **14,** 125–142 (1981).
[46] S. K. Maiti and R. A. Smith, Comparison of the criteria for mixed mode brittle fracture based on the preinstability stress–strain field. Part I: slit and elliptical cracks under uniaxial tensile loading. *Int. J. Fracture* **23,** 281–295 (1983).

[47] M. Rothman and D. S. Ross, Stresses in plates with cracks and notches. *Engineering, Lond.* **179,** 175–180 (1955).
[48] J. R. Dixon, Computed values of the elastic stresses around a crack in an infinite plate in tension. NEL report no. 12, National Engineering Laboratory, East Kilbride, Glasgow (1961).
[49] J. R. Dixon and J. S. Strannigan, Stress distribution and buckling in thin sheets with central slits, in *Fracture* 69, Proc. 2nd Int. Conf. on Fracture, Brighton, April 1969 (Edited by P. L. Pratt, E. H. Andrews, R. L. Bell, N. E. Frost, R. W. Nichols and E. Smith), pp. 105–118. Chapman & Hall (1969).
[50] A. Gilabert, P. Sibillot, D. Sornette, C. Vanneste, D. Maugis and S. Muttin, Buckling instability and pattern around holes or cracks in thin plates under tensile load. *Eur. J. Mech., A—Solids* **11,** 65–89 (1992).
[51] R. N. L. Smith, Second order terms and strain energy density for the angled crack problem. *Engng Fracture Mech.* **26,** 463–469 (1987).
[52] F. A. McClintock, Discussion "On the crack extension in plates under plane loading and transverse shear". *Trans. ASME, J. bas. Engng* **85D,** 525–527 (1963).
[53] F. Erdogan and G. C. Sih, On the crack extension in plates under plane loading and transverse shear. *Trans. ASME, J. bas. Engng* **85D,** 519–525 (1963).
[54] J. C. Williams and P. D. Ewing, Fracture under complex stress. The angled crack problem. *Int. J. Fracture Mech.* **8,** 441–446 (1972).
[55] I. Finnie and A. Saith, A note on the angled crack problem and the directional stability of cracks. *Int. J. Fracture* **9,** 484–486 (1973).
[56] C. W. Woo and L. H. Ling, On angled crack initiation under biaxial loading. *J. Strain Anal.* **19,** 51–59 (1984).

APPENDIX 1

Some useful relations between elliptical and Cartesian coordinates are given below.
Letting $X = x/c$, $Y = y/c$ and

$$\Delta = (X^2 + Y^2 + 1)^2 - 4X^2 = (X^2 + Y^2 - 1)^2 + 4Y^2, \tag{A1}$$

we have

$$\sinh^2 \xi = \tfrac{1}{2}(\sqrt{\Delta} + X^2 + Y^2 - 1) \tag{A2}$$

$$\sin^2 \eta = \tfrac{1}{2}[\sqrt{\Delta} - (X^2 + Y^2 - 1)] \tag{A3}$$

$$U = \cosh \xi \sin \eta = \operatorname{sign}(Y)\left[\frac{\sqrt{\Delta} - (X^2 - Y^2 - 1)}{2}\right]^{1/2} \quad \text{if} \quad Y \neq 0$$
$$= \pm\sqrt{(1 - X^2)} \quad \text{if} \quad Y = 0 \quad \text{and} \quad |X| < 1$$
$$= 0 \qquad\qquad \text{if} \quad Y = 0 \quad \text{and} \quad |X| \geqslant 1 \tag{A4}$$

$$V = \sinh \xi \cos \eta = \operatorname{sign}(X)\left[\frac{\sqrt{\Delta} + X^2 - Y^2 - 1}{2}\right]^{1/2} \tag{A5}$$

$$\cosh 2\xi = X^2 + Y^2 + \sqrt{\Delta} \tag{A6}$$

$$\sinh 2\xi = [(X^2 + Y^2 + \sqrt{\Delta})^2 - 1]^{1/2} \tag{A7}$$

$$\cos 2\eta = X^2 + Y^2 - \sqrt{\Delta} \tag{A8}$$

$$\sin 2\eta = \operatorname{sign}(XY)[1 - (X^2 + Y^2 - \sqrt{\Delta})^2]^{1/2} \quad \text{if} \quad XY \neq 0. \tag{A9}$$

With

$$\frac{1}{\lambda} = 2 \sinh \zeta \sinh \bar{\zeta} = \cosh 2\xi - \cos 2\eta \tag{A10}$$

we obtain

$$\Delta = 1/4\lambda^2 \tag{A11}$$

$$2\lambda(\cosh 2\xi - 1) = 1 + \frac{X^2 + Y^2 - 1}{\sqrt{\Delta}}. \tag{A12}$$

Intermediate results for the computation of eqs (23)–(27) are

$$\sinh \bar{\zeta} \cosh \zeta = \tfrac{1}{2}(\sinh 2\xi - i \sin 2\eta) \tag{A13}$$

$$\sinh \bar{\zeta} \cosh \bar{\zeta} = \tfrac{1}{2}(\sinh 2\xi \cos 2\eta - i \cosh 2\xi \sin 2\eta) \tag{A14}$$

$$\sinh^2 \bar{\zeta} = \tfrac{1}{2}(\cosh 2\xi \cos 2\eta - 1 - i \sinh 2\xi \sin 2\eta) \tag{A15}$$

$$\varphi'(z) = \frac{\sigma}{4}\left[n\, e^{2\xi_0} e^{2i\beta} + (m - n\, e^{2\xi_0} e^{2i\beta}) \frac{\cosh \zeta}{\sinh \zeta}\right] \tag{A16}$$

$$\bar{z}\varphi''(z) = 2\sigma\lambda^3(m - n\, e^{2\xi_0} e^{2i\beta}) \sinh^3 \bar{\zeta} \cosh \bar{\zeta} \tag{A17}$$

$$\chi''(z) = -2\sigma\lambda^2[n\, e^{2\xi_0} \cosh 2(\zeta - \xi_0 - i\beta)] \sinh^2 \bar{\zeta}$$
$$+ 2\sigma\lambda^3[m \cosh 2\xi_0 - n \cos 2\beta + n\, e^{2\xi_0} \sinh 2(\zeta - \xi_0 - i\beta)] \sinh^3 \bar{\zeta} \cosh \zeta. \tag{A18}$$

(*Received* 28 *November* 1990)